elevated fields, consistent with the evolution of the $M(T)$ peak as a function of field [section C of (*17*)].

Figure 4 describes a possible scenario for the two stages of transitions. Below T_{AF}, the Néel order develops. We speculate that the growth of the Néel order parameter m_{AF} is arrested as the temperature is lowered past T_{hyb}, due to the onset of the nuclear spin order. A diminished m_{AF} would place the electronic phase in the regime close to the QCP that underlies the pure electronic system in the absence of any hyperfine coupling. This quantum criticality effectively induced by the nuclear spin order at zero magnetic field would naturally lead to the development of a superconducting state [section I of (*17*)]. As inferred from the experimental results (Fig. 1C), fluctuations of the A phase are already set in near T_B and lead to a substantial reduction of the staggered magnetization and the emergence of superconducting fluctuations well above the A-phase ordering temperature [section I of (*17*)].

The large initial slope of the superconducting upper critical field $B_{c2}(T)$ at $T_c \simeq 25$ T/K, extracted from both shielding (Fig. 3, inset) and Meissner measurements (fig. S3C), corresponds to an effective charge-carrier mass of several hundred m_e (where m_e is the rest mass of the electron), which implies that the superconducting state is associated with the Yb-derived 4f electrons (heavy-electron superconductivity). Extrapolating the positions of the low-temperature fc $M(T)$ peak to zero temperature, the critical field of the A phase $B_A = B(T_A \rightarrow 0)$ is found to be 30 to 60 mT, which corresponds to $g_{eff} = k_B T_A(B = 0)/\mu_B B_A = 0.03$ to 0.06 (where k_B is the Boltzmann constant and μ_B is the Bohr magneton). This value of g_{eff} is much smaller than the in-plane electronic g-factor 3.5 (*24*) but is a factor of 20 to 40 larger than in case of a purely nuclear spin ordering transition. We can understand this g_{eff} if the ordered moment is a hybrid of the electronic and nuclear spins with, at most, 2% of the ordered moments being associated with the 4f electron–derived spins.

The very large entropy near $T_A \geq 2$ mK is one of the most pronounced features in our observation. An alternative possibility for this entropy is the involvement of a "nuclear Kondo effect"—that is, the formation of a singlet state between the nuclear and conduction electron spins. The resulting superheavy fermions may be assumed to form Cooper pairs and cause a superconducting transition at $T_c \approx 2$ mK that would be probed by the magnetic and specific-heat measurements. Though our estimates of the nuclear Kondo temperature and the quasi-particle effective mass reveal discrepancies with this picture [section E of (*17*)], further theoretical and experimental work is needed to investigate the possible role of the nuclear Kondo effect in generating superconductivity in $YbRh_2Si_2$.

It is likely that the coupling of electronic and nuclear spin orders, as well as the concomitant emergence of new physics, is not exclusive to $YbRh_2Si_2$ [section H of (*17*)]. Systematic studies of other heavy-electron antiferromagnets at ultralow temperatures are needed to find out whether a hybrid electronic-nuclear order is a more general phenomenon. In addition, a comparative study would be highly welcome to evaluate whether superconductivity is truly absent in isotopically enriched $YbRh_2Si_2$ without Yb-derived nuclear spins, similar to the compound studied in (*25*).

Our ultralow-temperature measurements on the unconventional quantum critical material $YbRh_2Si_2$ reveal heavy-electron superconductivity below $T_c = 2$ mK. This observation strongly supports the notion that superconductivity near an AF instability is a robust phenomenon.

REFERENCES AND NOTES

1. P. A. Lee, N. Nagaosa, X.-G. Wen, *Rev. Mod. Phys.* **78**, 17–85 (2006).
2. H. Löhneysen, A. Rosch, M. Vojta, P. Wölfle, *Rev. Mod. Phys.* **79**, 1015–1075 (2007).
3. P. Gegenwart, Q. Si, F. Steglich, *Nat. Phys.* **4**, 186–197 (2008).
4. N. D. Mathur *et al.*, *Nature* **394**, 39–43 (1998).
5. O. Stockert *et al.*, *Nat. Phys.* **7**, 119–124 (2011).
6. J. Custers *et al.*, *Nature* **424**, 524–527 (2003).
7. H. Shishido, R. Settai, H. Harima, Y. Ōnuki, *J. Phys. Soc. Jpn.* **74**, 1103–1106 (2005).
8. T. Park *et al.*, *Nature* **440**, 65–68 (2006).
9. G. Knebel, D. Aoki, J.-P. Brison, J. Flouquet, *J. Phys. Soc. Jpn.* **77**, 114704 (2008).
10. H. Löhneysen *et al.*, *Phys. Rev. Lett.* **72**, 3262–3265 (1994).
11. A. Schröder *et al.*, *Nature* **407**, 351–355 (2000).
12. S. Paschen *et al.*, *Nature* **432**, 881–885 (2004).
13. S. Friedemann *et al.*, *Proc. Natl. Acad. Sci. U.S.A.* **107**, 14547–14551 (2010).
14. Q. Si, S. Rabello, K. Ingersent, J.-L. Smith, *Nature* **413**, 804–808 (2001).
15. P. Coleman, C. Pépin, Q. Si, R. Ramazashvili, *J. Phys. Condens. Matter* **13**, R723–R738 (2001).
16. T. Senthil, M. Vojta, S. Sachdev, *Phys. Rev. B* **69**, 035111 (2004).
17. Supplementary materials are available on *Science* Online.
18. E. Schuberth, M. Tippmann, C. Krellner, F. Steglich, *Phys. Stat. Solidi B* **250**, 482–484 (2013).
19. F. Steglich *et al.*, *Phys. Rev. Lett.* **43**, 1892–1896 (1979).
20. A. Steppke *et al.*, *Phys. Stat. Solidi B* **247**, 737–739 (2010).
21. H. M. Rønnow *et al.*, *Science* **308**, 389–392 (2005).
22. K. Andres, E. Bucher, P. H. Schmidt, J. P. Maita, S. Darack, *Phys. Rev. B* **11**, 4364–4372 (1975).
23. L. Steinke *et al.*, *Phys. Rev. Lett.* **111**, 077202 (2013).
24. J. Sichelschmidt, V. A. Ivanshin, J. Ferstl, C. Geibel, F. Steglich, *Phys. Rev. Lett.* **91**, 156401 (2003).
25. G. Knebel *et al.*, *J. Phys. Soc. Jpn.* **75**, 114709 (2006).

ACKNOWLEDGMENTS

We thank K. Andres, P. Coleman, P. Gegenwart, S. Paschen, and S. Wirth for useful discussions. Part of the work at the Max Planck Institute for Chemical Physics of Solids was supported by the Deutsche Forschungsgemeinschaft Research Unit 960 "Quantum Phase Transitions." Q.S. was supported by NSF grant DMR-1309531 and Robert A. Welch Foundation grant C-1411. E.S., Q.S., and F.S. thank the Institute of Physics, Chinese Academy of Sciences, Beijing, for hospitality. Q.S. and F.S. acknowledge partial support from the NSF under grant 1066293 and the hospitality of the Aspen Center for Physics. We declare no competing financial interests.

SUPPLEMENTARY MATERIALS

www.sciencemag.org/content/351/6272/485/suppl/DC1
Materials and Methods
Supplementary Text
Figs. S1 to S9
References (*26*–*65*)

23 February 2015; accepted 16 December 2015
10.1126/science.aaa9733

GEOPHYSICS

Periodic slow slip triggers megathrust zone earthquakes in northeastern Japan

Naoki Uchida,[1]* Takeshi Iinuma,[2]† Robert M. Nadeau,[3] Roland Bürgmann,[4] Ryota Hino[1]

Both aseismic and seismic slip accommodate relative motion across partially coupled plate-boundary faults. In northeastern Japan, aseismic slip occurs in the form of decelerating afterslip after large interplate earthquakes and as relatively steady slip on uncoupled areas of the subduction thrust. Here we report on a previously unrecognized quasi-periodic slow-slip behavior that is widespread in the megathrust zone. The repeat intervals of the slow slip range from 1 to 6 years and often coincide with or precede clusters of large [magnitude (*M*) ≥ 5] earthquakes, including the 2011 *M* 9 Tohoku-oki earthquake. These results suggest that inherently periodic slow-slip events result in periodic stress perturbations and modulate the occurrence time of larger earthquakes. The periodicity in the slow-slip rate has the potential to help refine time-dependent earthquake forecasts.

Slow (or aseismic) slip is a process by which faults displace rocks like earthquakes do, but much more slowly and without generating seismic waves (*1*, *2*). Slow fault-slip events increase stress in adjacent areas and may trigger damaging earthquakes (*3*). Foreshocks are sometimes related to precursory slow slip (*4*–*6*), and some slow-slip events revealed by geodetic measurements are accompanied by seismicity rate changes (*7*). However, the relationship between large earthquakes and aseismic slip is not well understood because of the poor

detectability of small slow-slip events with geodetic measurements and the rare occurrence of large earthquakes. We understand that repeating earthquakes involve the rupture of small asperities in the fault zone as seismic slips keep up with aseismic fault creep (slow slip) on the surrounding surface (*8*) (Fig. 1). Repeating earthquakes provide a remote measure of both localized seismic slip and the surrounding rate of aseismic slip on a fault that greatly improves the spatiotemporal resolution of slow slip (*4*, *9*, *10*). In this study, we refer to repeating earthquakes as "repeaters" and invoke them as a form of subsurface creep meter (Fig. 1). Here we consider repeater time series and global positioning system (GPS) measurements from the northeastern (NE) Japan subduction zone to detect small temporal changes in the slow-slip rate. Major earthquakes, including the great 2011 Tohoku-oki earthquake [magnitude (*M*) 9.0], also occur on the offshore plate interface between the subducting Pacific and continental plates (Fig. 2A) (*1*, *4*, *11*–*13*).

We examined the seismic moments and recurrence intervals of 6126 repeaters belonging to 1515 separate sequences to detect interplate slip-rate fluctuations for a period of up to 28 years (*14*) (table S1). In the offshore and near-shore Sanriku areas (Fig. 2), the slow-slip rates are estimated from 162 and 91 repeater sequences, respectively, using a 0.5-year moving time window, with the average rates plotted at the center of each time window (*14*) (Fig. 1). The variations in slip rate ranged from 0 to 290% of the long-term interplate slip rate (*15*) (7.4 ± 0.2 cm/year) and showed strong periodicity. The amplitude of the inferred slip rate depends on the length of the analysis window and the scaling relationship used to estimate the slip amount, but the periodicity is not affected by these conditions (*14*).

We estimated the dominant periods of slow slip, based on spectral analysis, to be 3.0 ± 0.1 SD years for the offshore Sanriku area (Fig. 2B and fig. S4I) and 2.7 ± 0.6 years for near-shore Sanriku area (Fig. 2C and figs. S4J and S5) (*14*). Two large slip-velocity peaks in 1990 and 1992 could bias the spectral estimate of period in the offshore Sanriku area (Fig. 2B), but analysis excluding data before 1992 also shows a similar dominant period (fig. S4I). We compared the timing of $M \geq 5$ events (Fig. 2, B and C) to the regional slip rate. The magnitude threshold was chosen to ensure a complete catalog for our analysis period and a big enough sample of larger events. Clustering of $M \geq 5$ earthquakes in the high slip-rate periods is evident, especially in the offshore area (Fig. 2B). We fitted simple sinusoidal curves to the slip-rate changes to define the phase of the periodicity, finding that 6.2 and 3.3 times as many 1984–2011 $M \geq 5$ earthquakes occurred during the positive period of the best-fit sinusoids for the offshore and near-shore Sanriku areas, respectively (Fig. 2, B and C; fig. S6, C and D; and table S2). We calculated the excess number of $M \geq 5$ earthquakes for a range of periods and found that they decay away ±0.15 years from the best-fit periods we established from the repeater data (fig. S6). We showed a concentration of $M \geq 5$ earthquakes near the inferred slip-rate peak (fig. S7), using histograms of earthquake occurrence with respect to phase of the best-fit sinusoids. We found a similar correlation between periodic slow-slip rates and large earthquakes for most of the eight offshore areas where we documented the distribution of repeaters and earthquakes (fig. S2 and table S2).

When we applied declustering to the earthquake catalog with a range of declustering parameters, the number of excess earthquakes in the positive period of the best-fit sinusoids decreased (tables S3 and S4). Although the excess ratios for the offshore Sanriku area range from 2.0 to 2.8, those for the near-shore Sanriku area are systematically reduced to 1.2, suggesting that clusters associated with large earthquakes influence the result.

A possible explanation for the correlated periodicity (Fig. 2 and fig. S7) is that periodically occurring $M \geq 5$ events and their afterslip trigger the smaller repeaters. However, close inspection of the repeater activity and inferred slip-rate changes for the major slip pulses in 1989–1990 and 1992 in the offshore Sanriku area (Fig. 3A) shows that the repeater-inferred slow slip begins accelerating a few days before the mainshocks associated with the slip pulses (*16*). The precursory repeater activity is a common feature before $M \geq 5$, $M \geq 6$, and $M \geq 7$ earthquakes (mainshocks) in the offshore Sanriku area and most of the other study areas (figs. S8 and S9). The precursory repeater accelerations concentrate close to mainshock epicenters (figs. S10 and S11), suggesting

[1]Graduate School of Science and International Research Institute of Disaster Science, Tohoku University, 6-6, Aramaki-aza-aoba, Aoba-ku, Sendai 980-8578, Japan. [2]International Research Institute of Disaster Science, Tohoku University, 468-1, Aramaki-aza-aoba, Aoba-ku, Sendai 980-0845, Japan. [3]Berkeley Seismological Laboratory and Berkeley Institute for Data Science, University of California, Berkeley, 211 McCone Hall, Berkeley, CA 94720-4767, USA. [4]Berkeley Seismological Laboratory and Department of Earth and Planetary Science, University of California, Berkeley, 389 McCone Hall, Berkeley, CA 94720-4767, USA.
***Corresponding author. E-mail: naoki.uchida.b6@tohoku.ac.jp**
†Present address: Japan Agency for Marine-Earth Science and Technology, Yokohama, 236-0001, Japan.

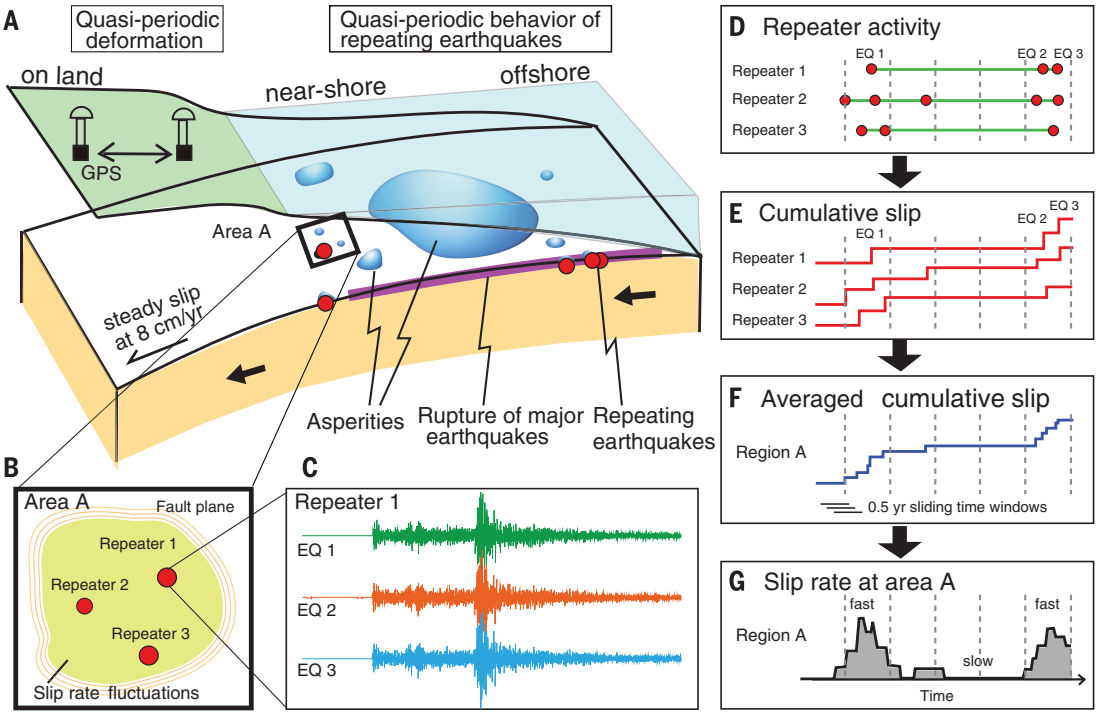

Fig. 1. Using repeaters to track slow plate-boundary slip. Schematic figure showing the tectonic setting (**A**), the activity of repeaters on the plate boundary (**B** and **C**), and steps to estimate the slip-rate time series from repeater data (**D** to **G**) (*14*). There are variably sized seismic patches on the plate boundary surrounded by aseismic slip areas (A). The small repeaters (C) represent repeated rupture of small patches that catch up with the creep in the surrounding areas (B). By calculating the slip of each earthquake, we obtain cumulative slip for each repeater sequence [(D) and (E)]. We average slip in each area (F) and obtain the temporal change of slip rate from the gradient of the averaged cumulative curve (G).

close interaction with the preceding repeater activity. Mainshocks are also generally followed by accelerated repeater activity (figs. S8 and S9), indicating rapid afterslip.

Marsan *et al.* (*17*) suggest occurrences of many slow-slip episodes in this subduction zone by discriminating normal from "abnormal" seismicity affected by transient loading. The activity of small repeaters indicates the involvement of spontaneous slow-slip events as the underlying aseismic loading process driving these episodic deformation transients. Observations from ocean-bottom pressure sensors of slow slip preceding M 6.1 and M 7.3 earthquakes occurring ~100 km south of this area in 2008 and 2011 (green stars in Fig. 2A) (*18*), respectively, are also consistent with this interpretation.

We tested the hypothesis of an ~3-year periodic slow slip promoting $M \geq 5$ earthquakes in the offshore Sanriku area by extrapolating the sinusoidal curve from the 1984 to 2011 slip-rate data back to 1930 (red curve in Fig. 3C). The positive phase of the sinusoidal curve (expected high–slip-rate periods) correlates with higher rates of $M \geq 5$ earthquakes back to around 1945 (Fig. 3C). The number of $M \geq 5$ earthquakes occurring during positive sinusoid amplitudes for the period 1956–1983 is about twice as high as the number of events occurring during negative sinusoid amplitudes (dashed curve in fig. S6C).

Our sinusoidal extrapolation of the slow slip assumes exact periodicity of the process, and slight shifts in the period result in large shifts in the timing of sinusoid peaks when extrapolating over many years. To address this, we examined the periodicity of the $M \geq 5$ declustered catalog using the Schuster spectrum (*19*). Our results show an ~3-year periodicity for the offshore Sanriku area (Fig. 3B) for all time spans considered, including the repeater analysis period. We do not find as strong a periodicity for the near-shore area (figs. S5A and S6D). Our

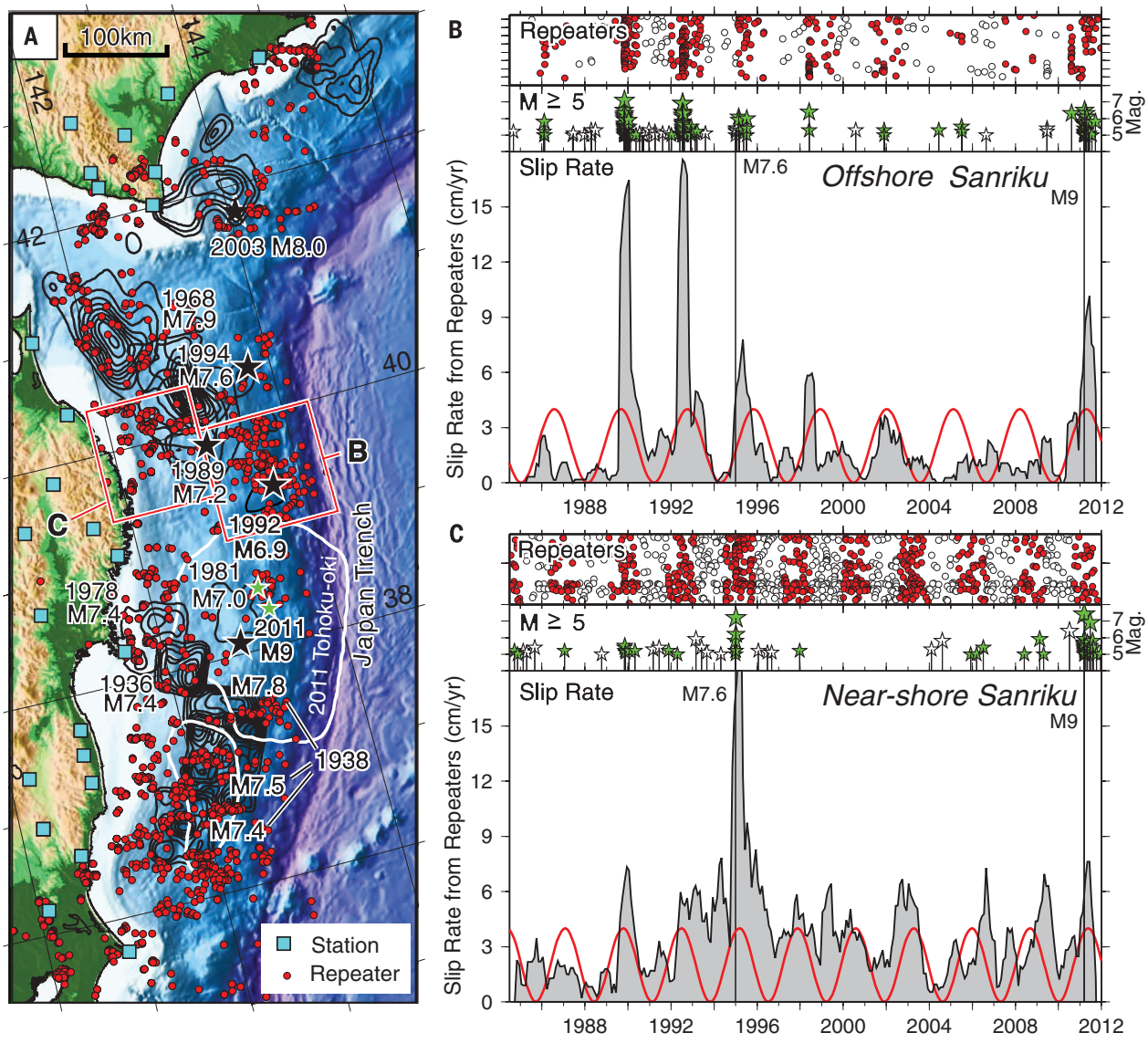

Fig. 2. Spatiotemporal distribution of repeaters and temporal variation of slow slip. (**A**) Distribution of repeater sequences (red circles) and slip areas of large earthquakes (black and white contours) (*11*–*13*, *29*, *30*). Cyan squares show seismic stations. Green stars show a M 6.1 earthquake in 2008 (north) and a M 7.3 earthquake in 2011 (south) that were preceded by slow slip (*18*). (**B** and **C**) Temporal distribution of repeaters near Sanriku aligned by latitude (top) (see fig. S1 for vertical enlargement), magnitude-time plot of $M \geq 5$ earthquakes (middle), and temporal change of slip rate inferred from repeaters (bottom) for offshore (B) and near-shore (C) areas off Sanriku shown in (A) (see fig. S3 for corresponding data for all other areas). Vertical lines show the times of the 1994 M 7.6 Sanriku-oki and the 2011 M 9 Tohoku-oki earthquakes. The number of $M \geq 5$ events in offshore and near-shore areas is 194 and 68, respectively. The red curves in (B) and (C) are best-fit sinusoidal functions fit to the slip-rate time series with 3.09- and 2.72-year periods, respectively. Repeaters and $M \geq 5$ events during the positive phase of the best-fitted sinusoid are shown by colored symbols, whereas those during the negative phase are shown by open symbols.

consideration of ~80 years of earthquakes offshore of Sanriku suggests that the periodicity of slow slip and associated larger earthquakes persists through time before the repeater analysis period.

Continuous GPS measurements across NE Japan provide complementary constraints on the time-variable coupling of the subduction thrust from the repeater data. The spatial gradient of observed displacement rates in the plate convergence direction reflects the strength of interplate locking and associated slip (*20*) (figs S12 and S13) (*14*), and its temporal variation may be a measure of the acceleration/deceleration of aseismic slip along the plate boundary. Although we infer that repeaters directly track slip on the subduction thrust, the on-land GPS data are only indirectly related to changing fault slip via elastic deformation. In order to stabilize the estimate of the time-dependent gradient of the displacement rate (the GPS gradient), we used a longer moving time window of 1 year. Periods of more negative GPS-gradient values, reflecting increased shortening, indicate times of stronger locking or lower slow-slip rates in the offshore area (fig. S12). The time series estimated from the observationally independent GPS gradient show similar fluctuations as those of the repeater slip rates (fig. S3).

We performed a moving spatial window analysis of the slip-rate spectrum to comprehensively examine the spatial distribution of the degree of periodicity and its dominant period along the NE Japan subduction zone. For each area, we determined the period of peak amplitude (short black vertical line in Fig. 3B) within the 1- to 9-year range and the degree of periodicity from the amplitude ratio of peak and average (red horizontal dashed line in Fig. 3B) amplitudes in the same period range. We used 0.4° (latitude) by 0.6° (longitude) spatial windows with 10 or more repeater sequences, showing widespread periodic behavior across the subduction zone (Fig. 4). The uncertainties of the estimated periodicities are generally on the order of 1 year (fig. S2B) (*14*). The dominant period has a heterogeneous distribution in both dip and strike directions (Fig. 4 and fig. S2A). Much of the subduction zone shows periods that range from 1 to 6 years and agrees with the periodicity of $M \geq 5$ earthquakes where strong slow-slip periodicity exists (fig. S2C). Around the slip areas of previous large earthquakes (*11*, *12*), including the 2011 Tohoku-oki earthquake (*13*), the aseismic slip rates are generally low and the periodicity is weak (light color in Fig. 4), with relatively long periods (>5 years). The relatively long period in the southern part of the coseismic slip area of the 2011 Tohoku earthquake (36.5° to 38°N) is consistent with a 5.9-year periodicity inferred from seismicity data for this area (*17*). The relatively weak periodicity near the large earthquakes may reflect the inhibition of periodic slip by strong interplate locking or indicate periods that are longer than the observation period.

The overall pattern of the offshore slip-rate periodicity from the repeater data correlates with the periods inferred from GPS gradients along profiles perpendicular to the margin (circles in Fig. 4 and fig. S13). A comprehensive evaluation of temporal slip-rate changes inferred from repeaters and GPS along the NE Japan subduction zone (figs. S2 to S4) shows correlations between the GPS gradients and near-shore repeater slip rates. The large variability in the correlations is probably due to the small-scale heterogeneities in periodic slow-slip behavior on the interplate fault in both along-dip and strike directions.

Periodic fault behavior may be driven by external forcing by tidal, atmospheric, and hydrologic cycles over a wide range of periods (*21*–*23*). However, we are unaware of forcing processes that recur at the most common periods we observe of 2 to 3 years (Fig. 4). Modeling

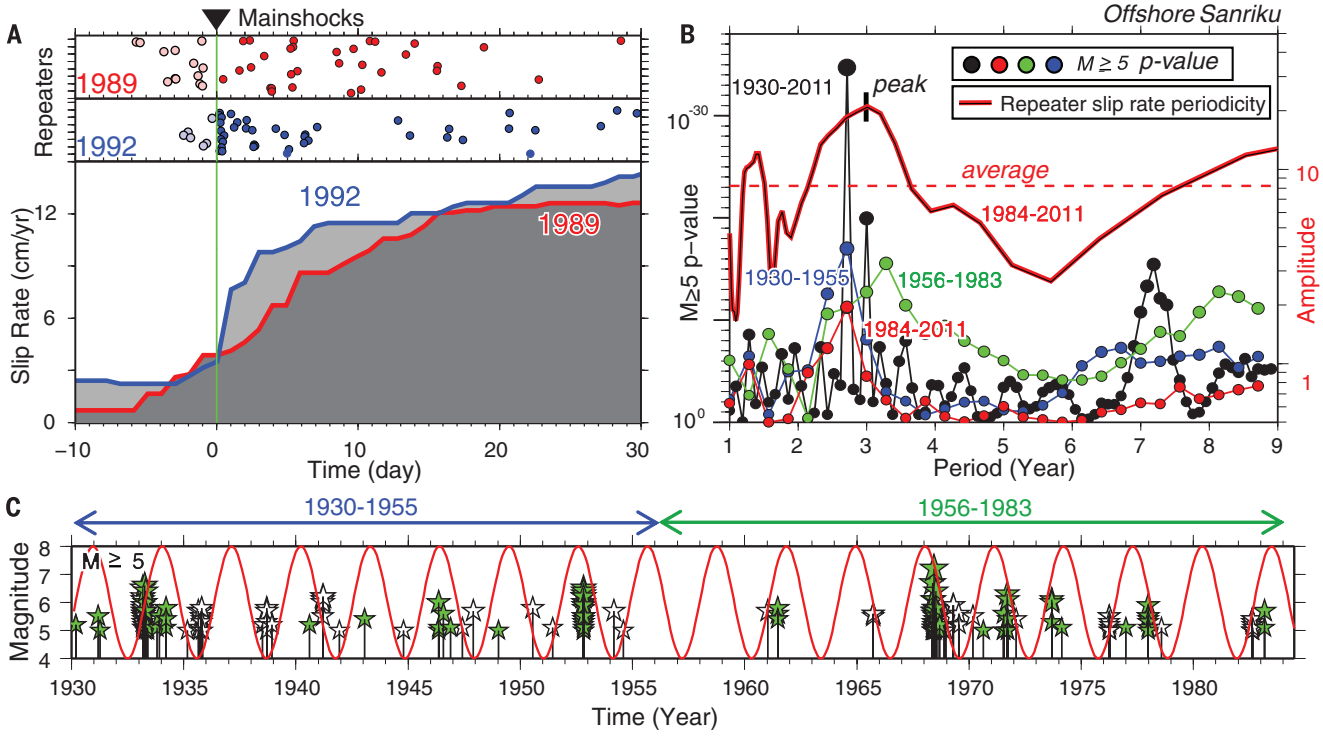

Fig. 3. Timing of repeaters, slow slip, and $M \geq 5$ earthquakes. (**A**) Times of the repeaters (top panels) and repeater-inferred slip rates (bottom panel) in the offshore Sanriku area (Fig. 2B) around the times of the 1989 M 7.2 (red) and 1992 M 6.9 (blue) mainshocks. Slip rates during 10 days before and 30 days after the mainshocks are plotted using a causal data window stepped every 1 day. Light and deep colors for the circles indicate repeaters before and after the mainshocks, respectively. (**B**) Amplitude spectrum of the slip rate for the offshore Sanriku area (red line; the original slip-rate time series is shown in Fig. 2B). The horizontal dashed red line shows the average of the amplitude in a 1- to 9-year period range. Black, red, green, and blue circles show Schuster spectra (*19*) for the $M \geq 5$ declustered earthquake catalogs for the time periods shown in the figure. The P values on the vertical axis give the probability of observing such a level of periodic variations in a catalog with a constant seismicity rate. (**C**) Magnitude-time plot of $M \geq 5$ earthquakes in the offshore Sanriku area before the repeater analysis period (i.e., 1930 to 1983). The red curve is the same sinusoidal function as in Fig. 2B, extrapolated from the fitting period. The green and white stars show events during times of positive and negative amplitude of the extrapolated sinusoid, respectively. Green and blue lines show the time period used in Fig. 3B. Plots similar to Fig. 3, B and C, but for the near-shore Sanriku area are shown in fig. S5, A and B, respectively.

studies suggest that slow-slip event periodicity may be governed by fault zone properties, including dilatancy, permeability, fluid pressure, and healing rates (*24*, *25*). Audet and Bürgmann (*26*) draw on the observed correlation of recurrence periods of deep slow-slip events in global subduction zones with seismic velocity variations to support a scenario of slow-slip event periodicity being governed by fault zone properties. The enduring nature of the periodic behavior we document suggests that fault zone constitutive properties could govern the recurrence of slow-slip events off northern Japan.

The 2011 Tohoku-oki earthquake occurred 0.7 years before the end of our analysis period. Slip rate peaks in the off-Sanriku areas before the 2011 Tohoku-oki earthquake, and the subsequent timing of the 2011 earthquake falls in the positive period of the sinusoidal slip-rate curve (Fig. 2, B and C), although the accelerations are not as obvious in the southern areas (fig. S3, E and F). Slow slip was detected in 2008 and 2011 from ocean-bottom pressure sensors (*18*) to the south of the off-Sanriku area. The slip episode appears to have triggered the largest foreshock (M 7.3) that occurred 2 days before the Tohoku-oki earthquake (*18*). Preseismic slow-slip migration toward the mainshock hypocenter occurred in February to March 2011 (*4*), but no significant preslip was detected on the megathrust fault immediately before the Tohoku-oki earthquake, from the analysis of seafloor vertical deformation data near the epicenter (*27*).

Large postseismic slip continues off Tohoku (*28*). If the inherent fault zone properties govern the periodicity of slow-slip transients, the periodicity may not change because of the Tohoku-oki earthquake. Previous examples support this scenario: The first slow-slip acceleration after the 1994 Sanriku-oki earthquake (M 7.6) that occurred just north of the Sanriku area (Fig. 2A) started somewhat earlier, but the period and phase did not change much for later slip accelerations in the offshore Sanriku area (Fig. 2B). In the case of the 2003 Tokachi-oki earthquake (M 8.0), the periodicity in the offshore area only became prominent after the earthquake (fig. S3C).

In most probabilistic earthquake forecasts based on recurrence intervals and time since the last event, a constant loading rate is implicitly assumed. The inherent periodicity of slow slip found in this study suggests that probabilistic forecasts of future earthquakes can be improved by explicitly considering cyclic loading-rate changes. The real-time monitoring of slow slip may also help improve the estimation of time-dependent earthquake hazards (*29*).

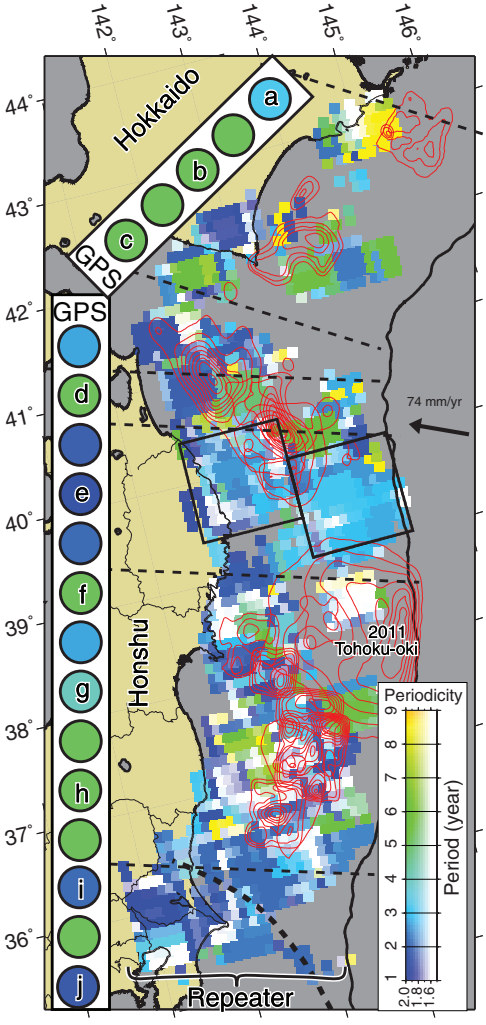

Fig. 4. Spatial distribution of degree of periodicity and dominant period estimated from the repeater data. The color intensity shows the degree of periodicity, and the colors show the dominant period for the periods from 1984 to 2011 (between 36.5° and 41.5°N) and from 1993 to 2011 (north of 41.5°N and south of 36.5°N). The periods indicated for each area represent the dominant peak in the amplitude spectrum of the slip-velocity variations inferred from repeaters for 0.4° (latitude) by 0.6° (longitude) spatial windows. Contours show slip areas for the 2011 Tohoku-oki earthquake (M 9.0) and other M 7 or larger earthquakes since 1930 (*11*–*13*, *30*). Colored circles show the dominant period of the on-land GPS gradient in plate motion parallel to the N105°E (Honshu) and N120°E (Hokkaido) directions (see fig. S13 for the spectrum of gradient time series in profile lines a to j that are used to compute the dominant periods).

REFERENCES AND NOTES

1. K. Heki, S. Miyazaki, H. Tsuji, *Nature* **386**, 595–598 (1997).
2. G. Dragert, K. Wang, T. S. James, *Science* **292**, 1525–1528 (2001).
3. P. Segall, A. M. Bradley, *Geophys. Res. Lett.* **39**, L18308 (2012).
4. A. Kato *et al.*, *Science* **335**, 705–708 (2012).
5. M. Bouchon, V. Durand, D. Marsan, H. Karabulut, J. Schmittbuhl, *Nat. Geosci.* **6**, 299–302 (2013).
6. S. Ruiz *et al.*, *Science* **345**, 1165–1169 (2014).
7. S. Ozawa, H. Suito, M. Tobita, *Earth Planets Space* **59**, 1241–1245 (2007).
8. R. M. Nadeau, T. V. McEvilly, *Science* **285**, 718–721 (1999).
9. R. M. Nadeau, T. V. McEvilly, *Science* **303**, 220–222 (2004).
10. N. Uchida, T. Matsuzawa, *Earth Planet. Sci. Lett.* **374**, 81–91 (2013).
11. Y. Yamanaka, M. Kikuchi, *Earth Planets Space* **55**, e21–e24 (2003).
12. Y. Yamanaka, M. Kikuchi, *J. Geophys. Res.* **109**, B07307 (2004).
13. T. Iinuma *et al.*, *J. Geophys. Res.* **117**, B07409 (2012).
14. Materials and methods are available as supplementary materials on *Science* Online.
15. G. F. Sella, T. H. Dixon, A. Mao, *J. Geophys. Res.* **107**, 2081 (2002).
16. N. Uchida, A. Hasegawa, T. Matsuzawa, T. Igarashi, *Tectonophysics* **385**, 1–15 (2004).
17. D. Marsan, T. Reverso, A. Helmstetter, B. Enescu, *J. Geophys. Res. Solid Earth* **118**, 4900–4909 (2013).
18. Y. Ito *et al.*, *Tectonophysics* **600**, 14–26 (2013).
19. T. J. Ader, J.-P. Avouac, *Earth Planet. Sci. Lett.* **377–378**, 97–105 (2013).
20. J. C. Savage, *J. Geophys. Res. Solid Earth* **88**, 4984–4996 (1983).
21. K. Heki, *Earth Planet. Sci. Lett.* **207**, 159–164 (2003).
22. Y. Tanaka, *Geophys. J. Int.* **196**, 760–787 (2014).
23. F. F. Pollitz, A. Wech, H. Kao, R. Bürgmann, *J. Geophys. Res. Solid Earth* **118**, 2445–2459 (2013).
24. Y. Liu, *Geophys. Res. Lett.* **40**, 1311–1316 (2013).
25. P. Segall, A. M. Rubin, A. M. Bradley, J. R. Rice, *J. Geophys. Res. Solid Earth* **115**, B12305 (2010).
26. P. Audet, R. Bürgmann, *Nature* **510**, 389–392 (2014).
27. R. Hino *et al.*, *Mar. Geophys. Res.* **35**, 181–190 (2014).
28. S. Ozawa *et al.*, *J. Geophys. Res.* **117**, B07404 (2012).
29. T. H. Jordan, L. M. Jones, *Seismol. Res. Lett.* **81**, 571–574 (2010).
30. T. Murotani, M. Kikuchi, Y. Yamanaka, "Rupture processes of large Fukushima-Oki earthquakes in 1938," paper S052-004, presented at the 2003 Japan Geoscience Union, Chiba, Japan, 2003.

ACKNOWLEDGMENTS

We thank Y. Yabe, T. Matsuzawa, W. Nakamura, R. C. Turner, S. Tanaka, C. W. Johnson, W. L. Ellsworth, Y. Ogata, and A. Hasegawa for fruitful discussion. The anonymous reviewers were helpful in greatly improving the manuscript. This work was supported in part by Japan Society for the Promotion of Science (JSPS) KAKENHI 23740328 and 15K05260 and the Ministry of Education, Culture, Sports, Science and Technology of Japan, under its Earthquake and Volcano Hazards Observation and Research Program. N.U. acknowledges support by Tohoku University under its Leading Young Researcher Overseas Visit Program. R.M.N. acknowledges support from the Berkeley Institute for Data Science, funded by the Moore-Sloan Data Science Environment Program. R.B. acknowledges support by U.S. NSF award EAR-1246850. R.H. acknowledges support by JSPS KAKENHI 26000002. The repeating earthquakes were selected based on the seismic waveforms from stations of Hokkaido University, Hirosaki University, Tohoku University, and the University of Tokyo. The repeating earthquake catalog is available as supplementary material on *Science* Online. The Japan Meteorological Agency (JMA) earthquake catalog used in this study is available at www.jma.go.jp, subject to the policies of the JMA. The GEONET F3 GPS solutions used in this study are available at www.gsi.go.jp, subject to the policies of the Geospatial Information Authority of Japan.

SUPPLEMENTARY MATERIALS

www.sciencemag.org/content/351/6272/488/suppl/DC1
Materials and Methods
Figs. S1 to S14
Tables S1 to S4
References (*31*–*42*)

26 August 2015; accepted 22 December 2015
10.1126/science.aad3108

www.sciencemag.org/content/351/6272/488/suppl/DC1

Supplementary Materials for

Periodic slow slip triggers megathrust zone earthquakes in northeastern Japan

Naoki Uchida,* Takeshi Iinuma, Robert M. Nadeau, Roland Bürgmann, Ryota Hino

*Corresponding author. E-mail: naoki.uchida.b6@tohoku.ac.jp

Published 29 January 2016, *Science* **351**, 488 (2016)
DOI: 10.1126/science.aad3108

This PDF file includes:

Other Supplementary Materials for this manuscript include the following:
(available at www.sciencemag.org/content/351/6272/488/suppl/DC1

Methods

Slip rate estimation from repeating earthquakes

We used Uchida and Matsuzawa (2013)'s catalogue (*10*) in which repeating earthquakes are selected based on waveform similarity. The waveform data used here are vertical component data from the microearthquake observation network of Hokkaido University, Hirosaki University, Tohoku University and the University of Tokyo (Fig. 2A). Most of the seismometers are of 1 Hz velocity type with sampling frequency of 100 Hz and for the period from 1984 to 2011 (36.5º – 41.5ºN) and 1993 to 2011 (to the south of 36.5º and to the north of 41.5ºN). The catalogue contains earthquakes larger than M2.5 before the Tohoku-oki earthquake and larger than M4.0 after the earthquake. This difference is because the earthquake catalogue is not complete for events smaller than M4.0 after the Tohoku-oki earthquake. Coherence of earthquake pairs for fixed time windows of 40 s from the P wave arrival that always include S phase arrivals, and these were evaluated to select repeating earthquakes. For earthquakes from M2.5 to M4.0, the similarity threshold is 0.95 for averaged coherencies in the 1 - 8 Hz band. For earthquakes larger than M4.0, we choose the frequency band around the corner frequency of the smaller event in the pair (1/2 to 2 times the corner frequency) and the coherence threshold is 0.8. The thresholds were determined based on the frequency distribution of coherence and the hypocenter locations of earthquakes determined precisely by waveform-based differential time data for the off-Kamaishi repeaters (*31*). The focal mechanisms of the repeating earthquakes are of low-angle thrust type (*10*), suggesting that they are occurring on the plate boundary.

After the selection of repeating earthquakes, the slip for each small repeating earthquake was estimated based on the following relationship between the seismic moment (Mo; dyne·cm) and fault slip (d; cm) (*32*)

$$\log(d) = -2.36 + 0.17\log(M_0) \qquad (1)$$

This empirical relationship was obtained from shallow repeating earthquake data in California. The seismic moment was estimated from the following relationship between the moment and magnitude (M) (*33*).

$$\log(M_0) = 1.5M + 16.1. \qquad (2)$$

The magnitude used here is determined by the Japan Meteorological Agency.

The periodicity or recurrence intervals of individual repeating earthquake sequences is sometimes studied to understand the nature of recurrent earthquakes (e.g., 34, 35). The repeating earthquakes are thought to be recurring in relatively regular intervals if the aseismic slip rate in the surrounding area is constant. In this study, however, we focus on time-varying aseismic slip that can be estimated from many repeating earthquake sequences. We estimate slip rates in each time period and area, estimated by dividing the cumulative slip by time and averaging all the repeating sequences in an area. The averaged slip rate expresses aseismic slip rate in the area and is not directly related to the recurrence intervals of each sequence if many repeating earthquakes are used for the averaging. In this study we used more than 10 sequences in the averaging process.

We estimated 0.5-year averaged slip rate stepping in 0.1-year intervals from all repeater sequences in each area. The choice of the averaging time window length (0.5 year) affects the estimated slip rate but does not strongly impact the inferred periodicity

(Fig. S14). The estimated slip rate is plotted at the center of each window. The use of different relationships between the magnitude and slip (eqs. 1 and 2) will yield a slightly different slip rate. Igarashi et al. (2003) (36) confirmed that the slip estimate from Nadeau and Johnson's relationship applied to the time intervals between repeating earthquakes close to the coast of northeastern Japan is consistent with the slip estimated from the long-term relative plate motion. Chen et al., (2007) (34) show that the relationship is applicable to Parkfield, NE Japan and eastern Taiwan. Mavrommatis et al (2015) (37) suggest similarly good fits to data for Beeler et al. (2001) (38)'s model and Nadeau and Johnson's model (32). Therefore, we consider Nadeau and Johnson's relationship fully appropriate for the slip estimate and the use of different relationships would not affect the inferred periodicity of slip-rate variation.

Figure 1 schematically shows the analyses steps described above. Suppose there are only three repeater sequences in area A (Fig. 1B). Note that the actual data has at least 10 sequences for the estimation of the spatial distribution of slip rate periodicity (Fig., 2, Fig. 4). Repeater sequence 1 has three earthquakes (EQ 1 – 3) whose waveforms are shown in Fig. 1C. Figure 1D illustrates the repeater activity showing the occurrence time of each earthquake by circles. This corresponds to the top figures of for real data shown in Figs. 2 B and C and Fig. S3. By calculating the slip of each earthquake with equation (1), we can obtain cumulative slip for each repeater sequence (Fig. 1E). By averaging the cumulative slip for the three repeater sequences, we obtain averaged cumulative slip estimates in area A (Fig. 1F). We consider this to reflect the temporal evolution of aseismic fault creep in area A. The temporal change of slip rate in area A is obtained from the gradient of the cumulative slip by using a 0.5-year sliding time window (Fig. 1G). This corresponds to the bottom figures for the real data shown in Figs. 2 B and C and Figs. S3.

The spectrum analyses and fitting of sinusoid to the observations are performed based on the final slip-rate time series. We consider only periods ranging from 1 – 9 years, constrained by the observation time period (28 years) and the smoothing window (0.5 year). In the sinusoid fitting, we seek optimum period yielding the largest cross-correlation-coefficient with changing period about the peak period of the slip-rate spectrum shown in Figs. S6A and S6B. We define the phase of the sinusoidal function so that it is positive when the function value exceeds the average. Note that the periods estimated from the two methods are slightly different but the differences are insignificant (Fig. S3 and Table S2).

Estimation of temporal change of the interplate coupling from GPS data

One of the major factors that determine horizontal ground velocity of the forearc area is interplate coupling (*20*, *39*). We estimated the temporal change in the interplate coupling along the subducting plate interface in NE Japan based on the spatial gradients of the surface displacement rates estimated from on-land GPS data (Fig. 1A). We assume most of the interplate locking occurs in the offshore region according to previous studies (*39*). If the interplate locking is strong, the surface landward deformation becomes larger towards the trench (Fig. S12A). This spatial difference in velocity can be expressed as a velocity gradient (Fig. S12C). If the locking ratio changes, the gradient changes (Figs. S12B and 12D). To estimate the temporal change of velocity gradient, we used daily site coordinate time series of GEONET (F3 solutions) that have been provided by the Geospatial Information Authority of Japan.

First, we extract displacement rates at each GPS station from the site coordinate time series by fitting a mathematical function that consists of long-term linear trend, annual and biannual trigonometric curve, and steps due to earthquakes and antenna replacements. We assign 5 year time windows ending every Monday from 24 March 1997 to 22 July 2013. For the long-term linear trends, we divides the 5-year window into five successive 1-year windows that the value at the junction of the 1-year time windows are continuous (i.e. polygonal line). We regarded the linear trend estimated for the latest 1-year time window as the average velocity at the time window. Note that first 4-year time windows are used for the estimation of annual and biannual trigonometric curve, and steps but not used for the final 1-year average velocity. Applying this time series fitting procedure for coordinate time series of all GPS stations, we can obtain weekly surface velocity field.

The gradient of the surface velocities is calculated for each 30-km-wide profile region configured along the plate convergence direction (Fig. S2A). Horizontal velocities are projected into this direction. Spatial gradients of the surface horizontal velocities are estimated with linear regression for velocities of GPS stations inside the region excluding the velocities that are estimated from the time series shorter than 1 year. In Figs. S12E-H, we show examples of GPS velocities and gradients for two periods. The two periods show contrasting velocity gradients that can be interpret as strongly (Figs. S12E and G) and weakly (Figs. 12F and H) locked (coupled) periods in the offshore plate boundary. Positive horizontal velocity gradients indicate that the closer to the Japan trench a particular point is, the larger its eastward (N105ºE) velocity is.

We performed synthetic tests using forward dislocation models for assumed interplate coupling distributions, and found that 1) a large negative horizontal velocity gradient corresponds to strong interplate coupling at shallow to intermediate depth (less than about 50 km in depth), and 2) the negative velocity gradient goes towards zero when the plate interface beneath the land is not coupled. Therefore, we can capture the temporal change in the interplate coupling on the plate interface offshore the Northeast Japan by monitoring the temporal change in the horizontal velocity gradient. The temporal change of the velocity gradient and its spectrum is shown in Fig. S13. The inferred periodicities shown by colored circles in Fig. 4 are the peak periods shown by green circles in Fig. S13.

The overall decreasing trend of GPS-gradient throughout the observation period in area D and near-shore Sanriku is probably due to the locking recovery (deceleration of postseismic slip) after the 1994 Sanriku-oki earthquake (M7.6, Fig. 2A) that occurred close to these area (*40*).

Estimation of slow-slip period and its uncertainty

The dominant period of slow slip is estimated from the peak of the spectrum of slip rate curve (Fig. 3B). The uncertainty of the peak is estimated by bootstrapping the repeater data to estimate slip rate curves as follows. Note that we have 10 or more repeater groups for the estimate of slip rates. We randomly select repeaters in each area allowing duplication and estimate peak period within 2 years of the original dominant period. The 2-year band is used to estimate the uncertainty of the main spectrum peak without the effect of secondary peaks. The random resampling is executed 300 times to obtain the

standard deviation of the peak period. We regard the standard deviation as the uncertainty of the dominant period.

Estimation of the earthquake number ratio in the positive and negative phase of sinusoidal curve fitted to the slip-rate changes

The earthquake number ratio of earthquakes in positive and negative period of the sinusoids fitted to the slip rate curve was simply estimated by counting earthquake number within the positive and negative phase. In addition to the original data, we counted the ratio for data from Reasenberg [1985]'(*41*)s declustering method (program cluster2000x) that identifies aftershocks based on a physical two-parameter model of the earthquake interaction process. We also check the stability by using a range of declustering parameters (Tables S3 and S4).

Supplementary Text

Supplementary figures 1 to 14

Supplementary figures referred in the Methods and main text are shown below.

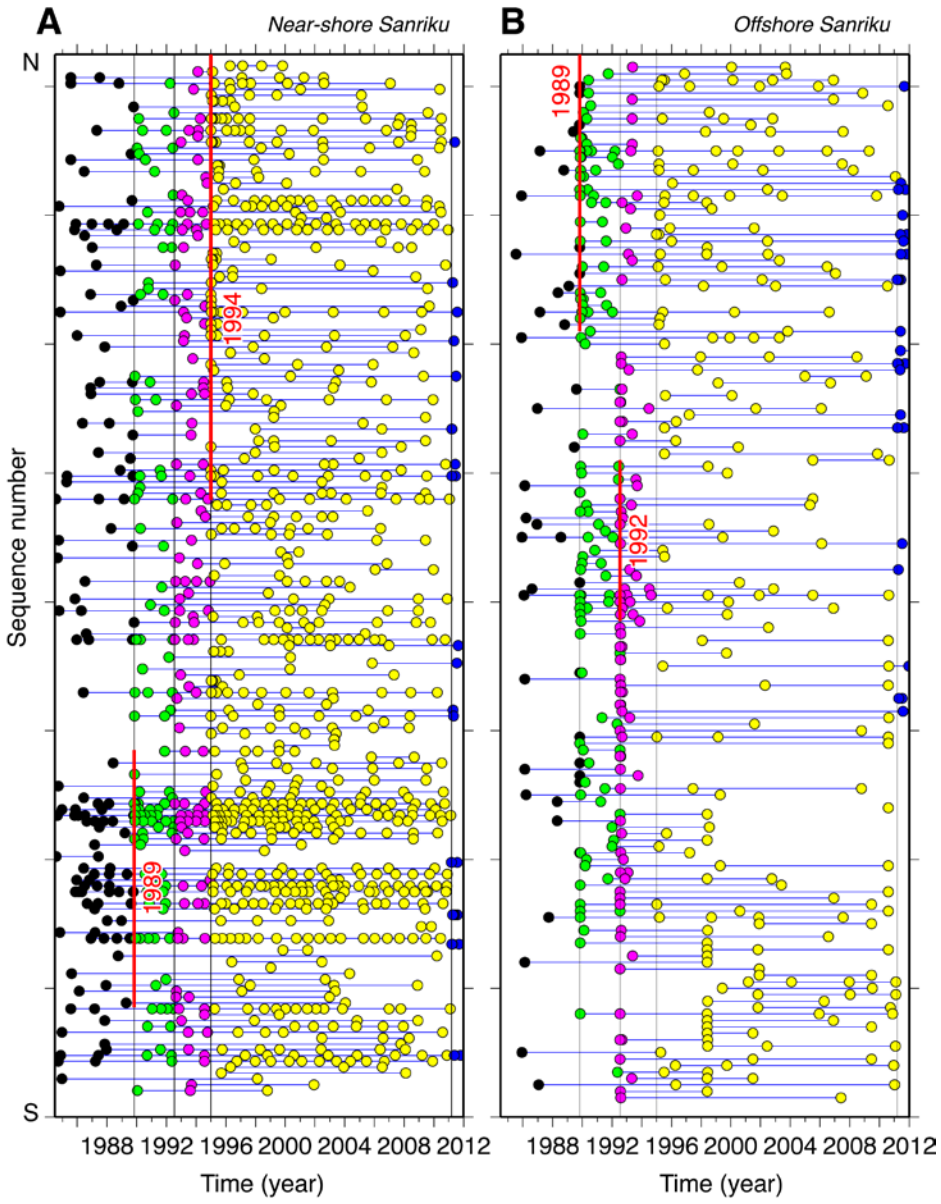

Fig. S1.

Temporal distribution of small repeating earthquakes for near-shore Sanriku (A) and offshore Sanriku (B) areas. The areas are shown in Fig. 2A. Circles show the occurrence time of each earthquake and horizontal lines connect the earthquakes that belong to the same sequence. Sequences are aligned from north to south. Vertical lines denote the occurrence times of the 1989 (M7.2), 1992 (M6.9) and 1994 (M7.6) Sanriku-oki earthquakes and the 2011 Tohoku-oki earthquake (M9.0) (See Fig. 2 for the epicenters). Red vertical lines show the approximate rupture extent of these events from Yamanaka and Kikuchi, 2004 (*12*). The circles are color-coded depending on the period between these earthquakes. Note that some of the repeating earthquakes occurred just before the four major earthquakes

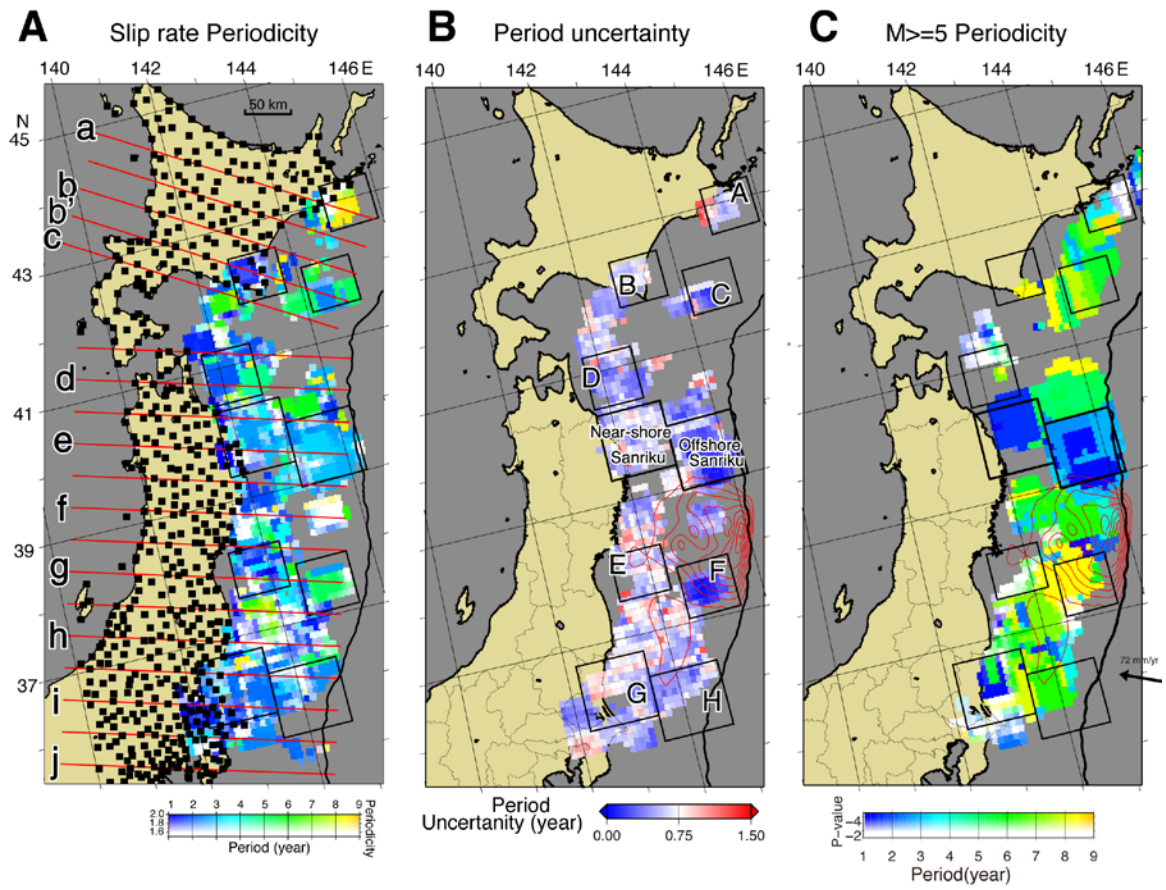

Fig. S2

(A) Map showing GPS stations (squares), profile lines of the GPS data analyses (red lines) and analyses area of the repeating earthquakes (black rectangles). Colors in the offshore area are the same as those on Fig. 4 (Spatial distribution of periodicity (color intensity) and dominant period (color) of interplate slip velocity estimated from small repeating earthquakes). (B) Uncertainty of periodicity that was estimated for repeater-derived slip-rate. (C) The distribution of dominant period (peak p-value) of M ≥ 5 earthquakes for the period from 1984 to March 11, 2011 (before the Tohoku-oki earthquake). The spatial window size is 0.8 degree (latitude) by 2.0 degree (longitude). The estimation was performed for areas 20 or larger M ≥ 5 earthquake exist.

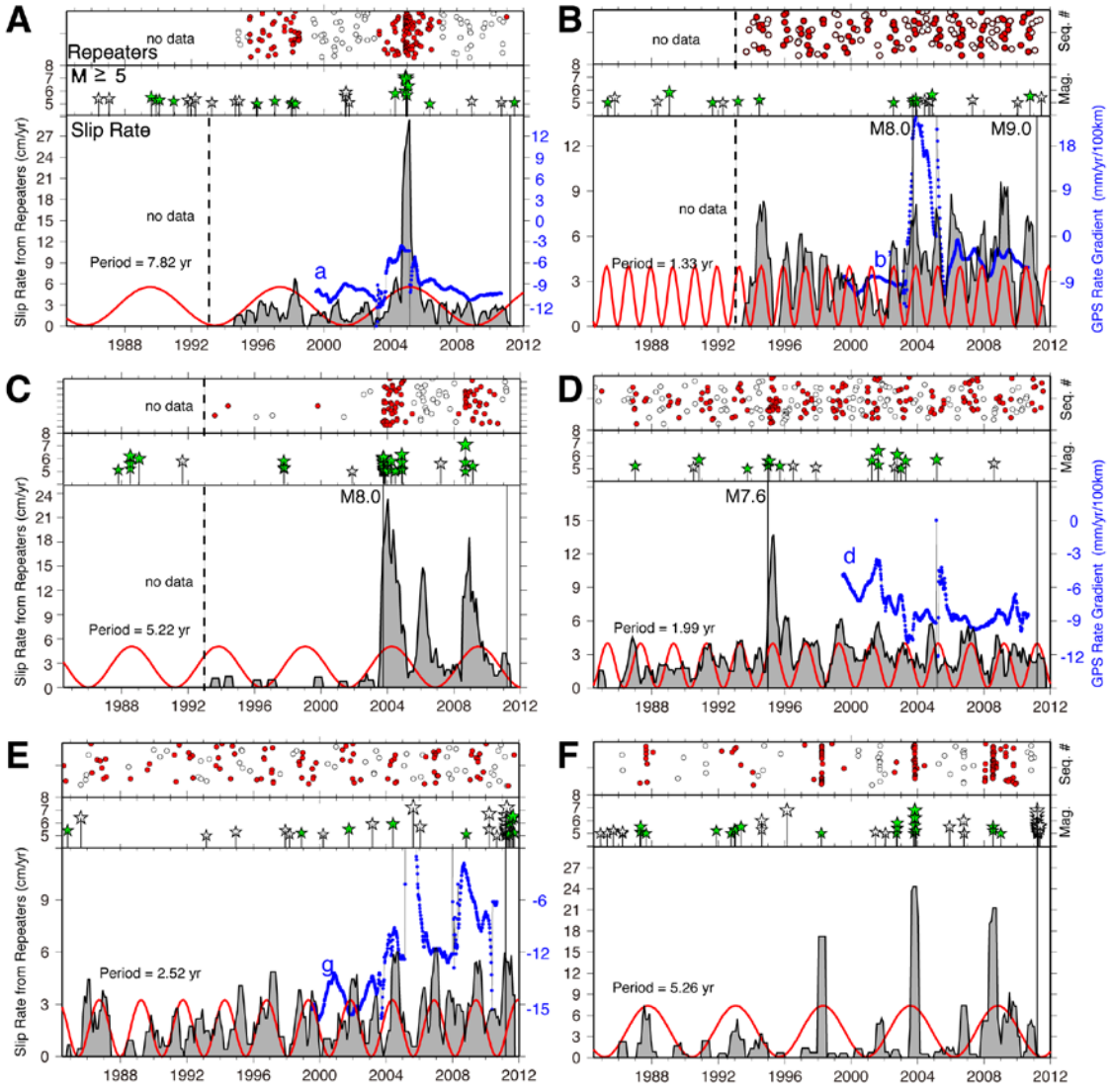

Fig. S3

Temporal distribution of small repeating earthquakes (top), magnitude-time plot of M ≥ 5 earthquakes (middle) and temporal change of slip rate inferred from repeating earthquakes (bottom) for areas A-H that are shown in Fig. S2 and offshore (I) and near-shore Sanriku (J) areas. Vertical lines show the times of the 1994 Sanriku-oki (M7.6), 2003 Tokachi-oki (M8.0) and the 2011 Tohoku-oki (M9.0) earthquakes. Red curves are sinusoidal functions fit to the slip rate changes. The best-fit periods are shown in each panel. The colored and white symbols for repeating earthquakes and M ≥ 5 earthquakes show events during times of positive and negative amplitude of the sinusoid, respectively. Blue lines show temporal change of horizontal land velocity gradient estimated from on-land GPS stations for near-shore areas. Note that the GPS velocity gradient scales are shown in blue on the right and analysis profiles are shown in Fig. S2A).

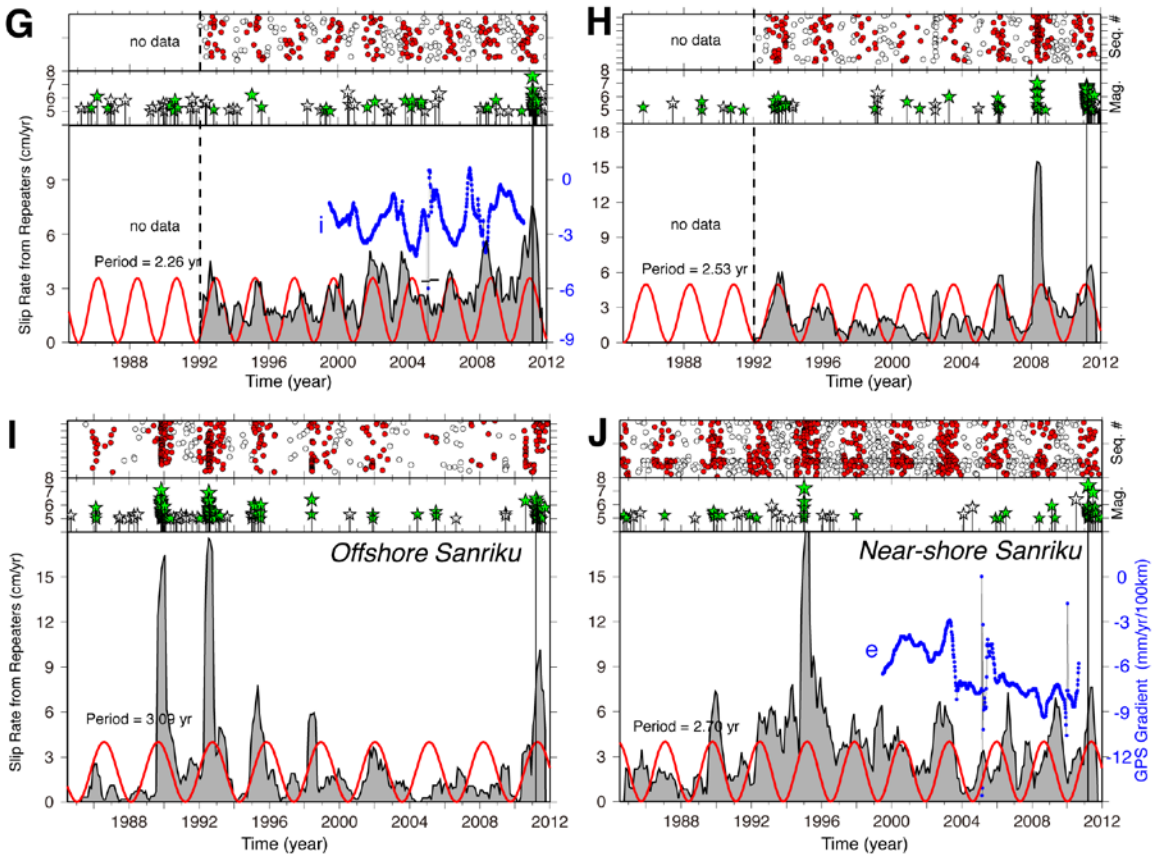

Fig. S3 (continue)

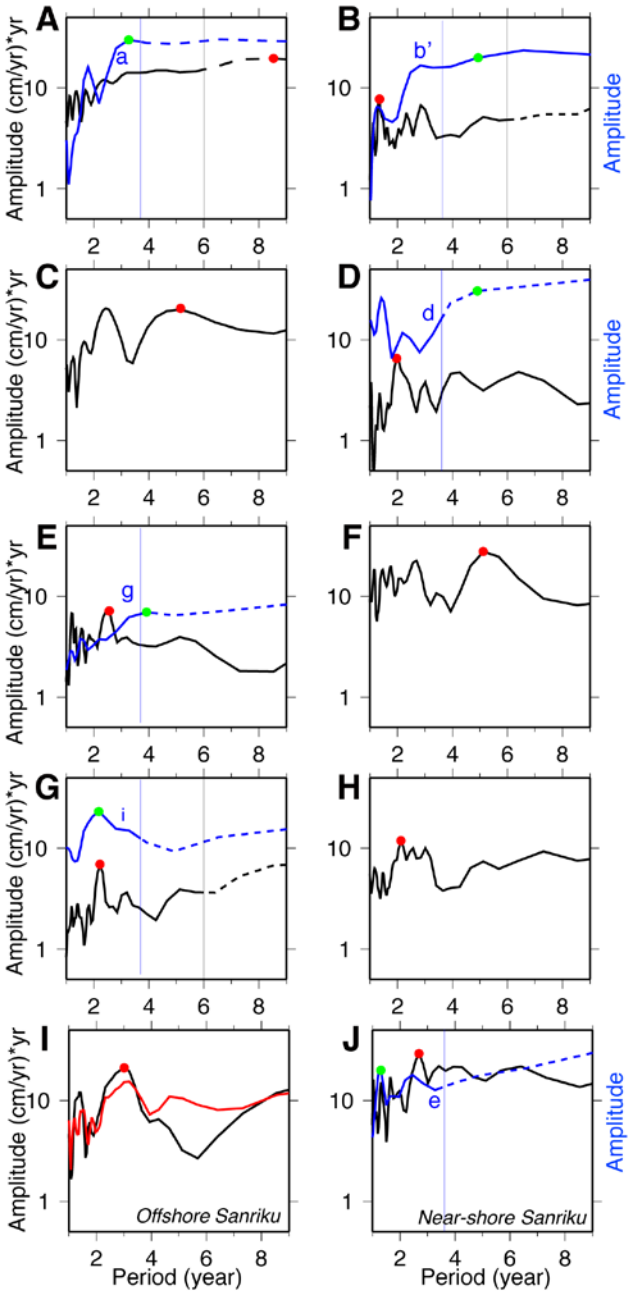

Fig. S4

Amplitude spectra of slip-rate time series for areas A-H shown in Fig. S2 and offshore Sanriku, near-shore Sanriku areas shown in Fig. 2A. The original slip-rate time series are shown in Fig. S3 and Figs. 2B, C. Red line in (I) shows spectrum for a limited period from 1992 to 2011 to exclude two large earthquakes in 1989 and 1992. Also shown with a blue line is the amplitude spectra of GPS gradient shown in Fig S3. Red and green dots show the peak of the amplitude spectrum in each panel. Dashed lines show spectra for the periods that are not constrained by 3 or more cycles. Note that the GPS data span 11 years, while the repeater data period is 19 or 28 years long.

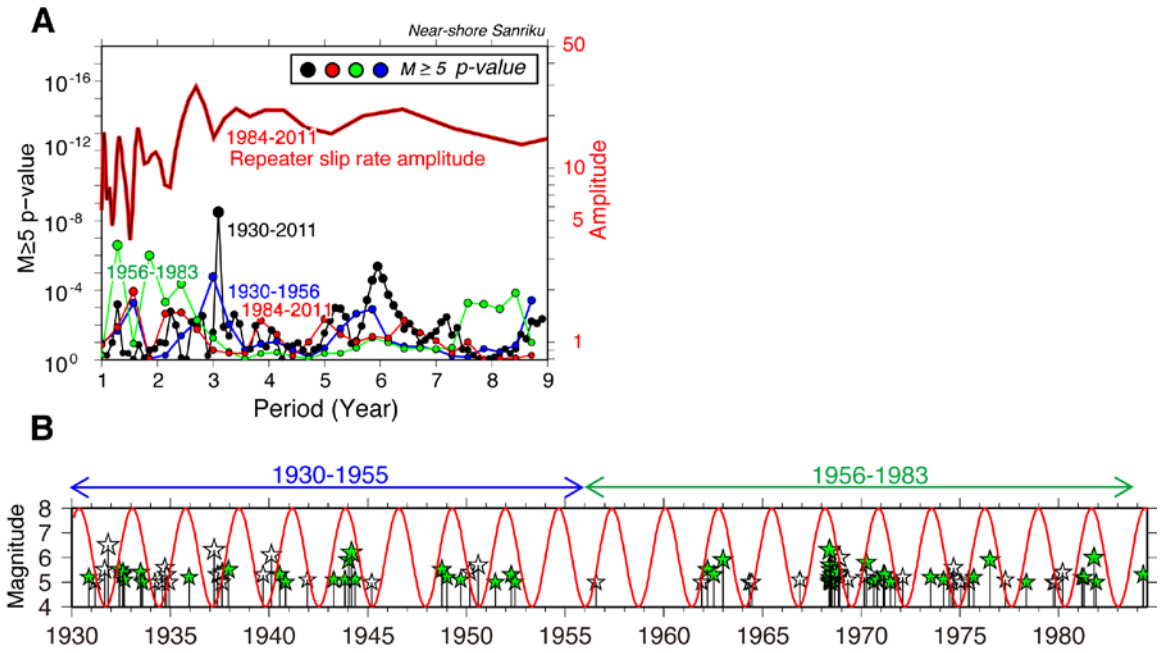

Fig. S5

(A) Schuster spectra (*19*) for M ≥ 5 earthquakes in the near-shore Sanriku area for four time periods shown in the figure (black, red, green, and blue circles). Amplitude spectrum of the slip rate from the repeating earthquake data is also shown by red line. (B) Magnitude vs. time plot of M ≥ 5 earthquakes in the near-shore Sanriku area for the period before the repeater analysis period (from 1930 to 1983). Red curve is the same sinusoidal function as in Fig. 2C that is extrapolated back in time from the original fitting range. Green and blue bidirectional arrows show the time periods used in Fig. S5A.

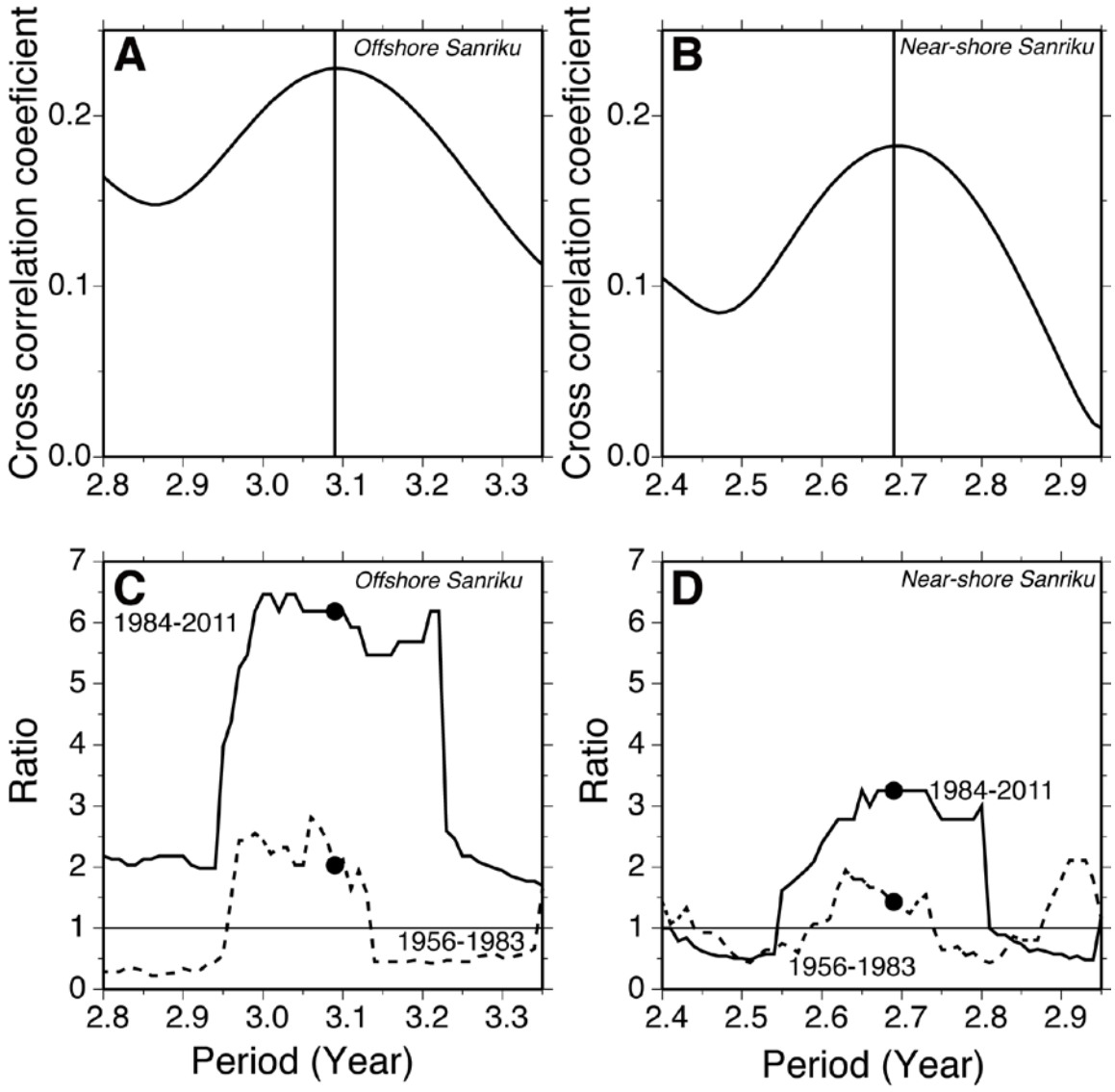

Fig. S6

Periodic slip rate and occurrence of M ≥ 5 earthquakes. (A and B) Cross-correlation-coefficient between the sinusoidal function and the slip-rate time series for a range of periods around that estimated from the spectral analyses for offshore Sanriku (A) and near-shore Sanriku (B) areas. (C and D) The ratio of M ≥ 5 earthquake number in positive phase of the sinusoidal curve fitted to the slip velocity to the number in negative phase for a range of periods. (C) and (D) are for the offshore and near-shore Sanriku, respectively. Black and dashed curves are for the period from 1984 to 2011 and 1956 to 1983, respectively. Black dots show the ratio for the period with the largest cross-correlation-coefficient.

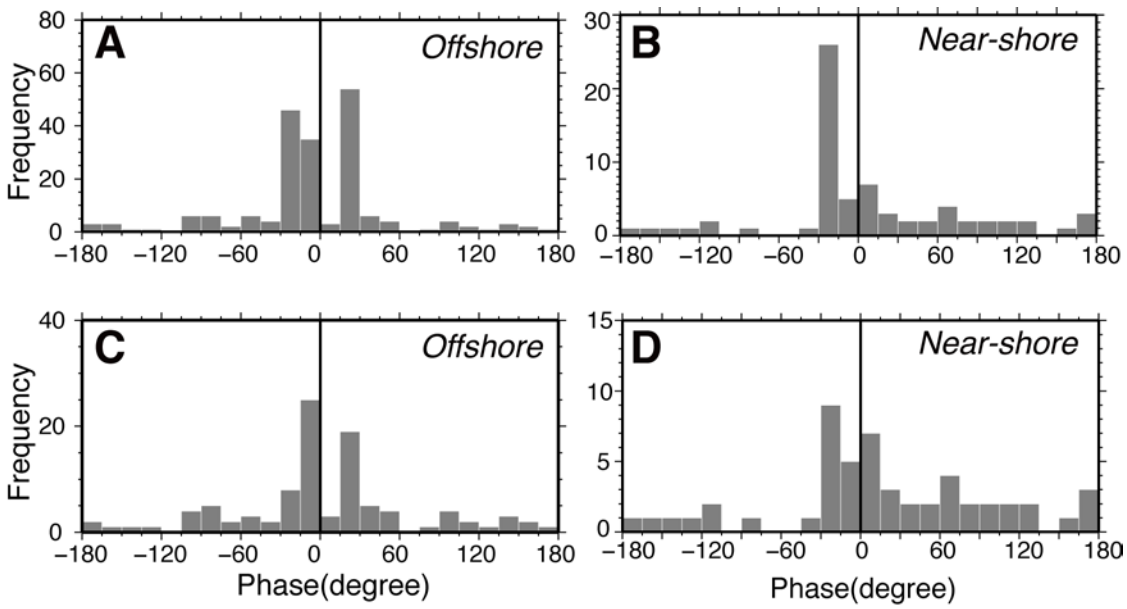

Fig. S7

Frequency distribution of M ≥ 5 earthquakes for each 15 degree bin of the phase of the sinusoidal curve fitted to repeater-derived slip rate for offshore and near-shore Sanriku, respectively. (A, B) original catalogue, (C, D) declustered catalogue by using Reasenberg's method. The phase zero is the peak of sinusoidal curve.

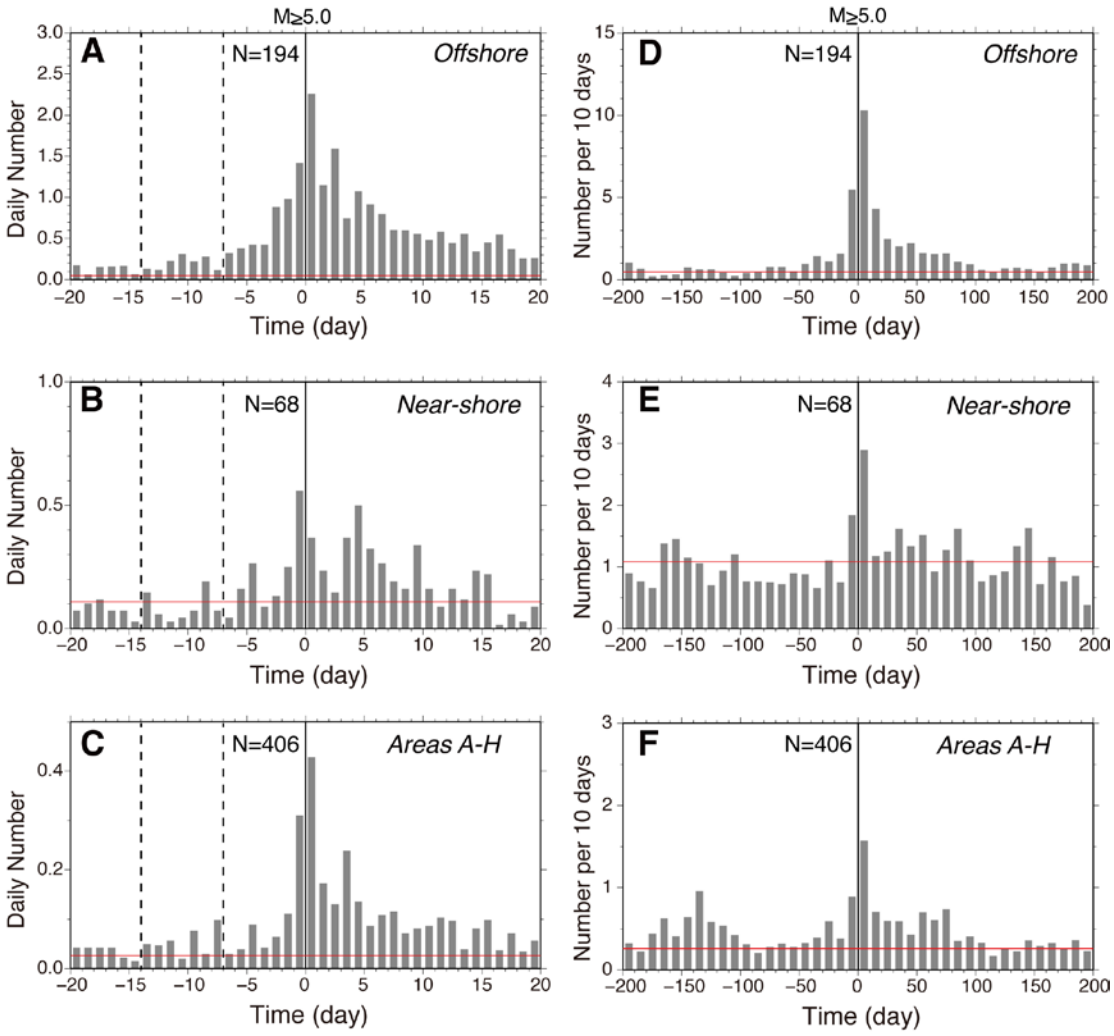

Fig. S8

Frequency distribution of repeating earthquakes before and after M≧5 mainshocks. The frequency is normalized by the number of mainshocks considered. (A-C) Daily number for offshore Sanriku, near-shore Sanriku and areas A-H shown in Fig. S2B. (D-F) The same but showing the number of repeaters per 10-day intervals over ± 200 days from the mainshocks. Vertical lines at zero denote the time of M≧5 earthquakes and the total number of mainshocks considered (*N*) is shown near the line. Vertical dashed lines mark three pre-mainshock periods for which spatial distribution of repeaters are shown in Figs S10 and S11. Horizontal red lines denote average daily (A-C) and 10 day (D-F) number of repeating earthquakes (normalized by *N*) in the whole analysis period.

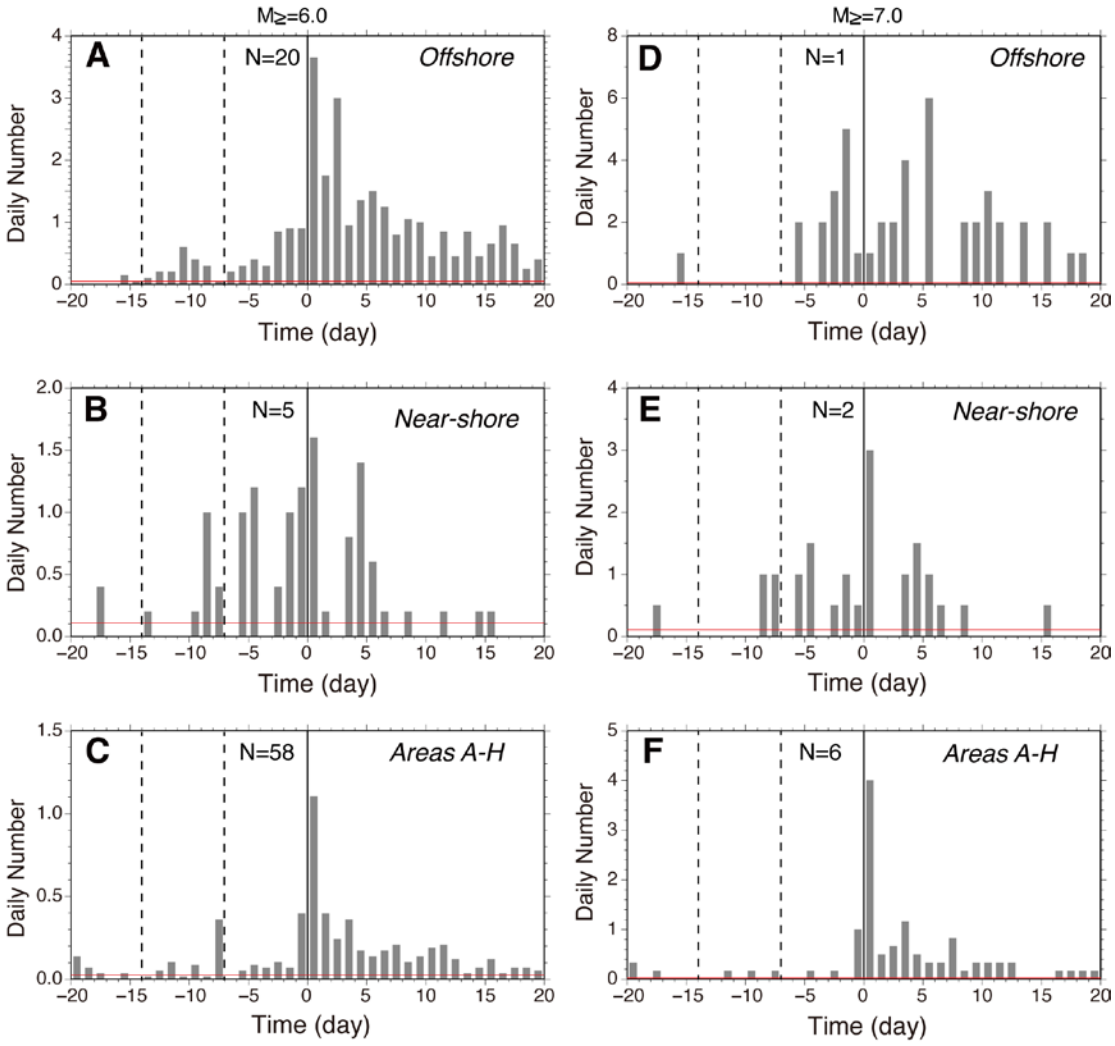

Fig. S9

Frequency distribution of repeating earthquakes before and after M≧6 (A-C) and M≧7 (D-F) mainshocks for offshore Sanriku, near-shore Sanriku and areas A-H. Daily numbers are shown. Other symbols are the same as Fig S8.

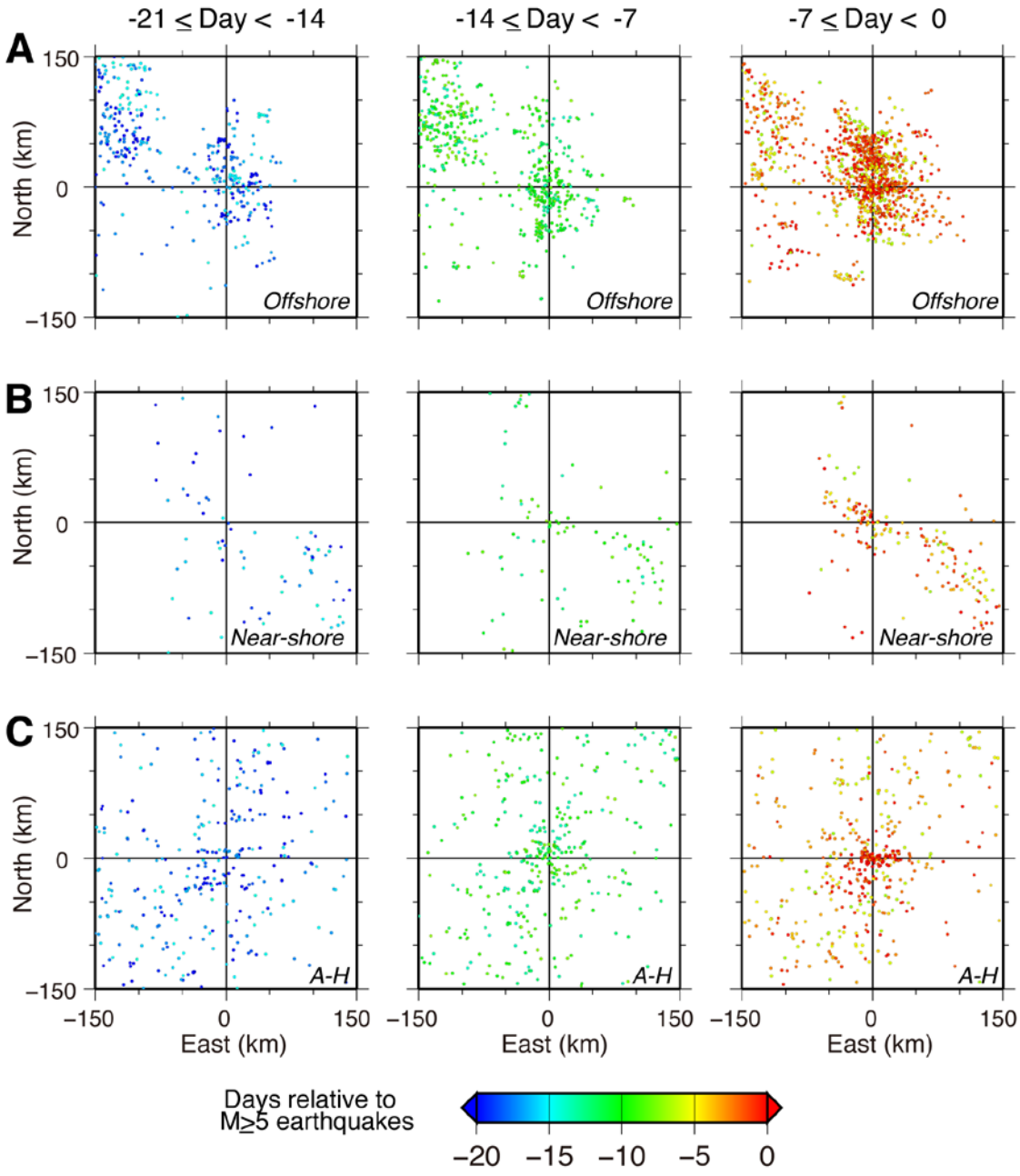

Fig. S10

Spatial distribution of repeating earthquakes relative to the epicenter of M ≧ 5 earthquakes in offshore Sanriku area (A), near-shore Sanriku area (B) and areas A-H (C) before the M≧5 earthquakes. Left, middle and right columns show the distribution in 21 to 14 days, 14 to 7 days and 7 to 0 days before the M≧5 mainshock earthquakes, respectively. The color of circles show the relative time to the M ≧ 5 mainshock earthquakes. The total number of mainshocks considered for each area are provided in Fig. S9.

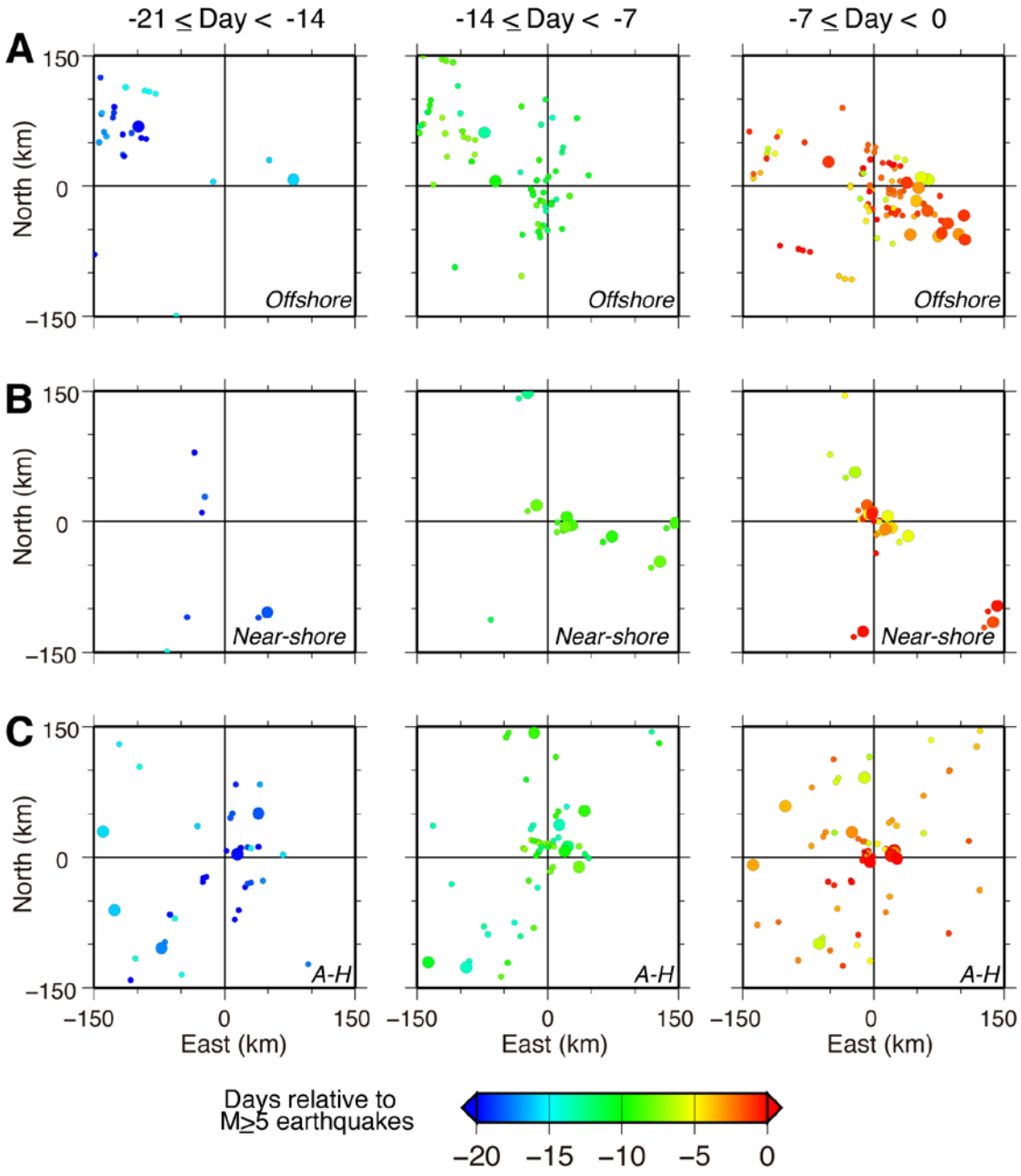

Fig. S11

Spatial distribution of repeating earthquake relative to the epicenter of M≧6 (small circles) and M≧7 (large circles) mainshock earthquakes in offshore Sanriku area (A) near-shore Sanriku area (B) and areas A-H (C). Left, middle and right columns show the distribution in 21 to 14 days, 14 to 7 days and 7 to 0 days before the mainshock earthquakes, respectively. The color of circles shows the relative time before mainshocks. The total number of mainshocks considered for each area are provided in Fig. S9.

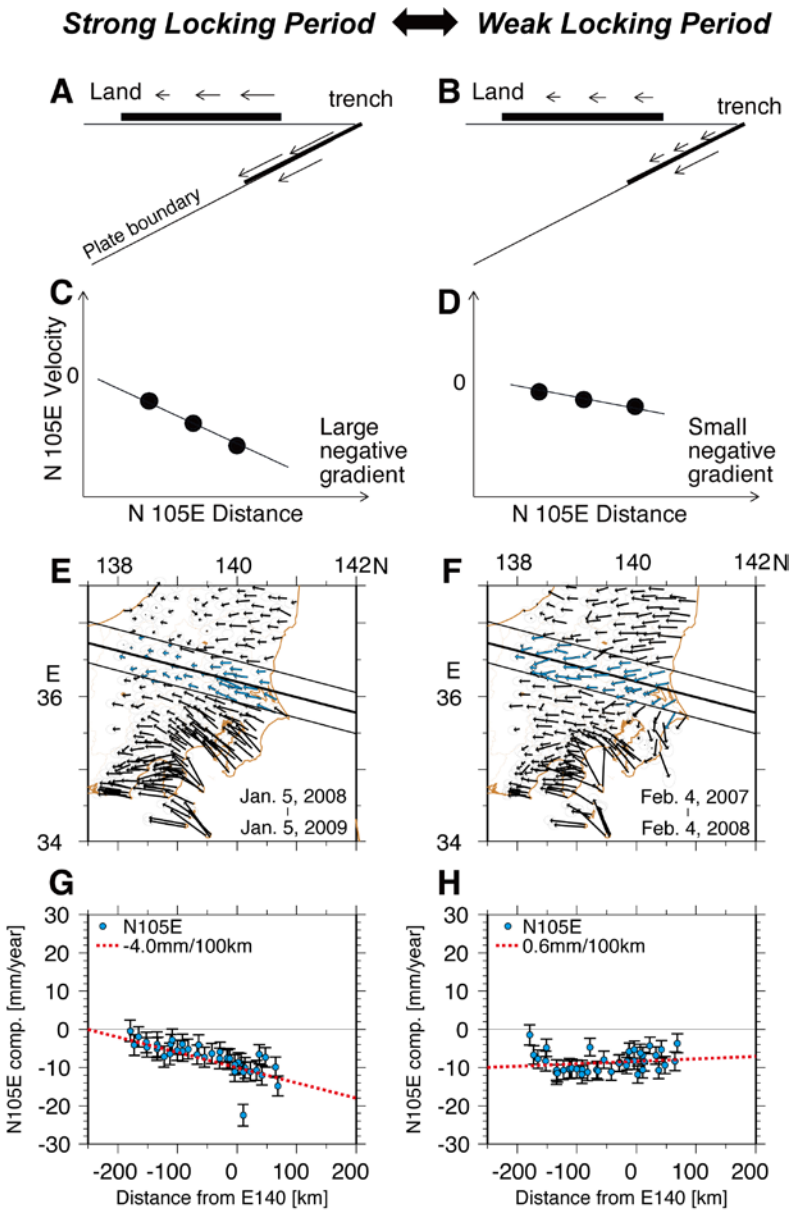

Fig. S12

Relationship between GPS-gradient and interplate locking. Left panels show strong locking period and right panels show weak locking period. (A) and (B) Schematic figures showing the interplate locking and surface deformation. (C) and (D) Schematic figures showing the relationship between distance along the subducting direction and horizontal ground velocity in subduction direction. (E) and (F) Examples of observed horizontal GPS velocity vectors offshore Ibaraki for the 1-year periods, starting from January 5, 2008 and February 4, 2007, respectively. (G) and (H) Examples of observed relationship between distance along the subducting direction (N105ºE) and horizontal ground velocity in the subduction direction for the periods shown in Figs (E) and (F), respectively. Each circle and error bars show velocity and its standard error, respectively.

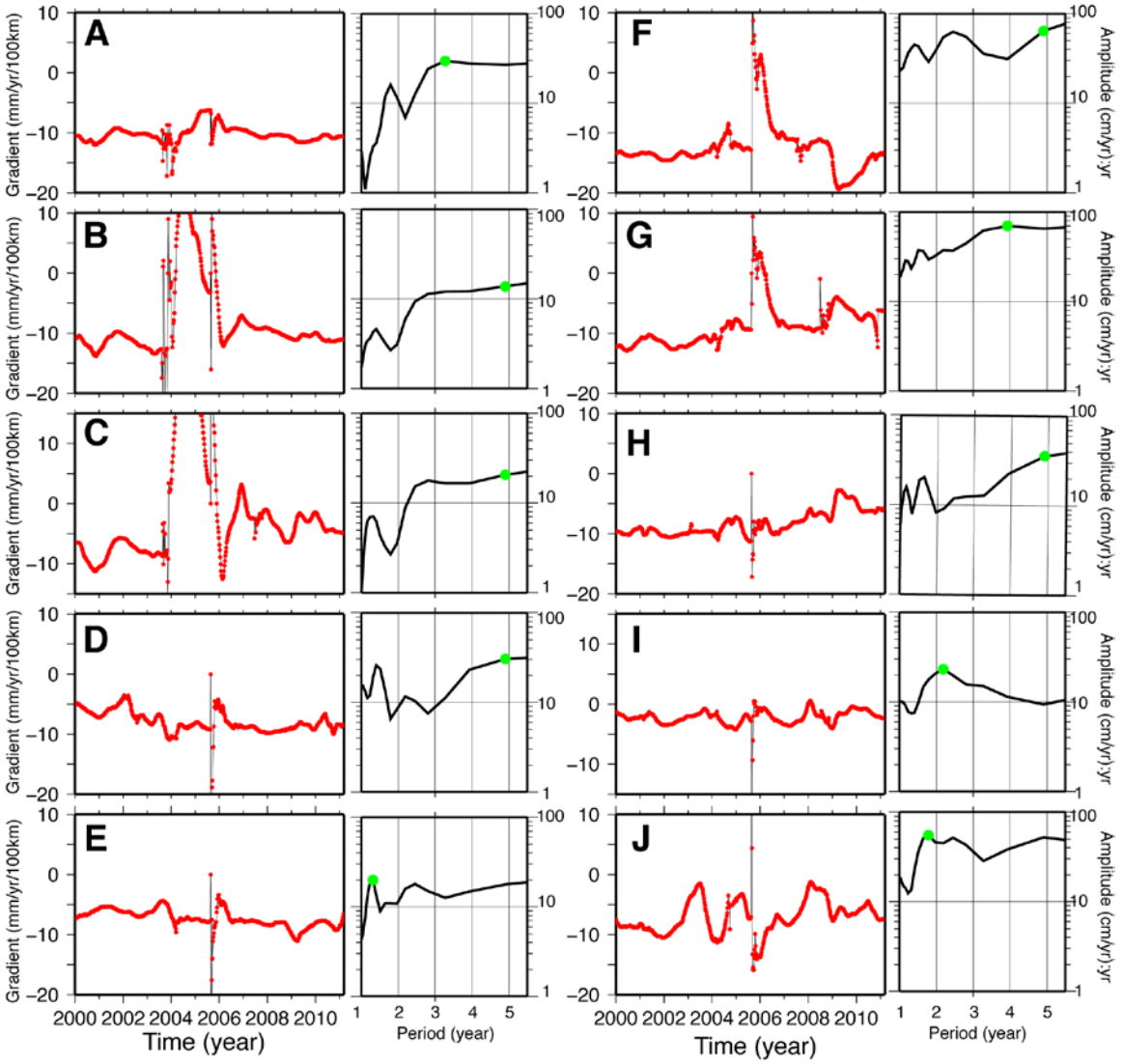

Fig. S13

Temporal change of the GPS velocity gradient and its spectra for profile lines a – j (A-J). The profile lines are shown in Fig. S2A. The disturbance around 2005 in a – j and around 2003-2004 in a – c are due to the M7.2 Miyagi-oki and M8.0 Tokachi-oki earthquake, respectively. Green dots in the right panels show the peak amplitude of the spectra.

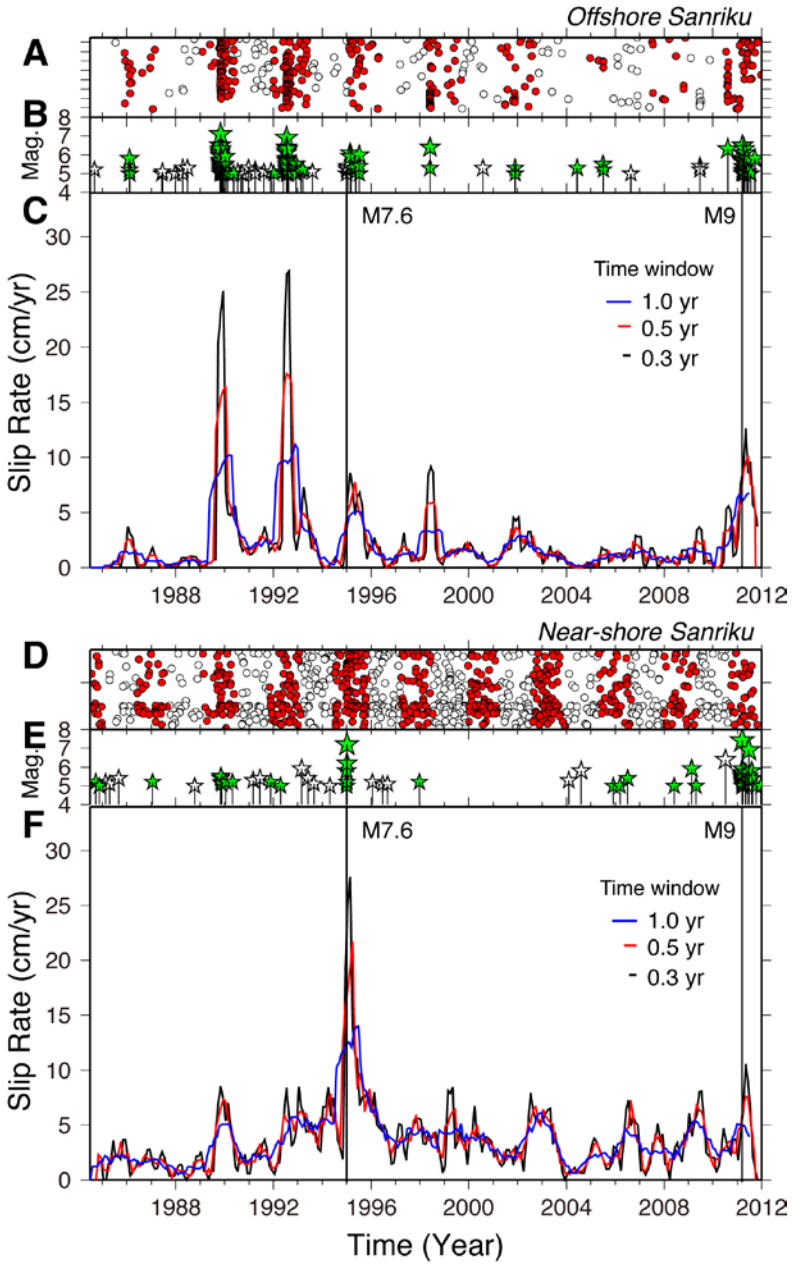

Fig. S14

Comparison of slip rate inferred from the analyses using different time-window lengths for offshore (A-C) and near-shore (D-F) Sanriku areas. Blue, red and black lines show slip rates from 1.0, 0.5 and 0.3 year time window analysis, respectively. Data are plotted at the center of each time window. Other panels are the same as Figs. 2B and C. The peak amplitudes depend on the time-window but the intervals between peaks and estimated periods do not change much.

Table S1 (separate file). The list of repeating earthquakes used in this study. The original data was reported by Uchida and Matsuzawa (2013) (*10*).

Table S2

Area	Period (year)	Uncertainty (year)	Number of Repeaters	N_{pos}/N_{neg} (Repeater)	Number of M≥=5 earthquakes	N_{pos}/N_{neg} (M≥5)	Probability [%] (M≥5) [1]
Offshore Sanriku	3.0	0.1	482	3.3	194	6.2	0.0
Near-shore Sanriku	2.7	0.6	1113	1.3	68	3.3	0.0
A	7.8	0.5	208	2.1	22	1.8	7.8
B	1.3	0.7	157	1.3	15	1.5	25
C	5.2	0.3	108	2.3	38	18	0.0
D	2.0	0.6	285	1.4	19	2.8	3.8
E	2.5	0.7	150	1.8	44	0.29	0.0
F	5.2	0.1	152	2.6	69	0.47	0.0
G	2.3	0.5	342	1.5	82	2.6	0.0
H	2.5	0.3	379	1.6	117	8.8	0.0

N_{pos} and N_{neg} mean number of earthquake in the positive and negative phase of sinusoid, respectively. For the N_{pos}/N_{neg} ratio, “inf” means the ratio is infinity (N_{neg} is zero) and “-“ means the number of earthquake in the magnitude range is zero. Earthquakes in the depth range from 0 to 90km are used.

[1] Probability of earthquakes occurring in the positive period than the observed value to be by random chance.

[2] Earthquakes within 20 km from the plate models of Slab 1.0 (*42*) are used to count earthquake number.

Table S2 (Continue)

Area	Number of M≥=4 earthquakes	N_{pos}/N_{neg} (M≥4)	Probability [%] (M≥4) [1]	Number of M≥=6 earthquakes	N_{pos}/N_{neg} (M≥6)	Probability [%] (M≥6) [1]
Offshore Sanriku	413	6.8	0.0	18	inf	0.0
Near-shore Sanriku	189	2.9	0.0	6	5.0	10
A	51	2.9	0.0	4	inf	4.5
B	42	1.6	6.2	0	-	-
C	85	9.6	0.0	5	inf	3.1
D	46	1.9	2.7	2	inf	27
E	125	0.42	0.0	10	0.43	4.7
F	190	0.36	0.0	10	0.25	0.4
G	254	2.7	0.0	10	2.3	22
H	243	6.6	0.0	17	16	0.0

Table S2 (Continue)

Area	Number of M≥=5 earthquakes [2]	N_{pos}/N_{neg} (M≥5) [2]	Probability [%] (M≥5) [1, 2]
Offshore Sanriku	176	6.7	0.0
Near-shore Sanriku	69	3.3	0.0
A	15	2.8	2.9
B	14	1.3	34
C	37	36	0.0
D	18	2.6	5.5
E	33	0.32	0.0
F	38	0.58	2.0
G	68	2.6	0.0
H	59	11	0.0

Table S3 Ratio of the number of earthquakes in the positive and negative phases of the sinusoid (Npos/Nneg) as a function of the choice of declustering parameters for offshore Sanriku area. Numbers in parentheses are total number of $M \geq 5$ events in declustered catalogs. P and Q are related to the duration of interaction period and size of interaction zone, respectively.

	Q		
P	20	30	50
0.50	2.8 (79)	2.8 (76)	2.8 (76)
0.90	2.1 (64)	2.0 (59)	2.0 (59)
0.99	2.6 (75)	2.5 (69)	2.5 (69)

Table S4 The same as Table S3 for near-shore Sanriku area.

	Q		
P	20	30	50
0.50	1.2 (53)	1.2 (53)	1.2 (53)
0.90	1.2 (46)	1.2 (46)	1.2 (46)
0.99	1.2 (53)	1.2 (53)	1.2 (53)

REFERENCES AND NOTES

1. K. Heki, S. Miyazaki, H. Tsuji, Silent fault slip following an interplate thrust earthquake at the Japan Trench. *Nature* **386**, 595–598 (1997). doi:10.1038/386595a0

2. G. Dragert, K. Wang, T. S. James, A silent slip event on the deeper Cascadia subduction interface. *Science* **292**, 1525–1528 (2001). Medline doi:10.1126/science.1060152

3. P. Segall, A. M. Bradley, Slow-slip evolves into megathrust earthquakes in 2D numerical simulations. *Geophys. Res. Lett.* **39**, L18308 (2012). doi:10.1029/2012GL052811

4. A. Kato, K. Obara, T. Igarashi, H. Tsuruoka, S. Nakagawa, N. Hirata, Propagation of slow slip leading up to the 2011 M_w 9.0 Tohoku-Oki earthquake. *Science* **335**, 705–708 (2012). Medline doi:10.1126/science.1215141

5. M. Bouchon, V. Durand, D. Marsan, H. Karabulut, J. Schmittbuhl, The long precursory phase of most large interplate earthquakes. *Nat. Geosci.* **6**, 299–302 (2013. doi:10.1038/ngeo1770

6. S. Ruiz, M. Metois, A. Fuenzalida, J. Ruiz, F. Leyton, R. Grandin, C. Vigny, R. Madariaga, J. Campos, Intense foreshocks and a slow slip event preceded the 2014 Iquique Mw 8.1 earthquake. *Science* **345**, 1165–1169 (2014). Medline doi:10.1126/science.1256074

7. S. Ozawa, H. Suito, M. Tobita, Occurrence of quasi-periodic slow-slip off the east coast of the Boso peninsula, Central Japan. *Earth Planets Space* **59**, 1241–1245 (2007). doi:10.1186/BF03352072

8. R. M. Nadeau, T. V. McEvilly, Fault slip rates at depth from recurrence intervals of repeating microearthquakes. *Science* **285**, 718–721 (1999). 10.1126/science.285.5428.718 Medline doi:10.1126/science.285.5428.718

9. R. M. Nadeau, T. V. McEvilly, Periodic pulsing of characteristic microearthquakes on the San Andreas fault. *Science* **303**, 220–222 (2004). Medline doi:10.1126/science.1090353

10. N. Uchida, T. Matsuzawa, Pre- and postseismic slow slip surrounding the 2011 Tohoku-oki earthquake rupture. *Earth Planet. Sci. Lett.* **374**, 81–91 (2013). doi:10.1016/j.epsl.2013.05.021

11. Y. Yamanaka, M. Kikuchi, Source process of the recurrent Tokachi-oki earthquake on September 26, 2003, inferred from teleseismic body waves. *Earth Planets Space* **55**, e21–e24 (2003). doi:10.1186/BF03352479

12. Y. Yamanaka, M. Kikuchi, Asperity map along the subduction zone in northeastern Japan inferred from regional seismic data. *J. Geophys. Res.* **109**, B07307 (2004). doi:10.1029/2003JB002683

13. T. Iinuma, R. Hino, M. Kido, D. Inazu, Y. Osada, Y. Ito, M. Ohzono, H. Tsushima, S. Suzuki, H. Fujimoto, S. Miura, Coseismic slip distribution of the 2011 off the

Pacific Coast of Tohoku Earthquake (M9.0) refined by means of seafloor geodetic data. *J. Geophys. Res.* **117**, B07409 (2012). doi:10.1029/2012JB009186

14. Materials and methods are available as supplementary materials on *Science* Online

15. G. F. Sella, T. H. Dixon, A. Mao, REVEL: A model for Recent plate velocities from space geodesy. *J. Geophys. Res.* **107**, 2081 (2002). doi:10.1029/2000JB000033

16. N. Uchida, A. Hasegawa, T. Matsuzawa, T. Igarashi, Pre- and post-seismic slip on the plate boundary off Sanriku, NE Japan associated with three interplate earthquakes as estimated from small repeating earthquake data. *Tectonophysics* **385**, 1–15 (2004). doi:10.1016/j.tecto.2004.04.015

17. D. Marsan, T. Reverso, A. Helmstetter, B. Enescu, Slow slip and aseismic deformation episodes associated with the subducting Pacific plate offshore Japan, revealed by changes in seismicity. *J. Geophys. Res. Solid Earth* **118**, 4900–4909 (2013). 10.1002/jgrb.50323 doi:10.1002/jgrb.50323

18. Y. Ito, R. Hino, M. Kido, H. Fujimoto, Y. Osada, D. Inazu, Y. Ohta, T. Iinuma, M. Ohzono, S. Miura, M. Mishina, K. Suzuki, T. Tsuji, J. Ashi, Episodic slow slip events in the Japan subduction zone before the 2011 Tohoku-Oki earthquake. *Tectonophysics* **600**, 14–26 (2013). doi:10.1016/j.tecto.2012.08.022

19. T. J. Ader, J.-P. Avouac, Detecting periodicities and declustering in earthquake catalogs using the Schuster spectrum, application to Himalayan seismicity. *Earth Planet. Sci. Lett.* **377-378**, 97–105 (2013).

20. J. C. Savage, A dislocation model of strain accumulation and release at a subduction zone. *J. Geophys. Res. Solid Earth* **88**, 4984–4996 (1983). doi:10.1029/JB088iB06p04984

21. K. Heki, Snow load and seasonal variation of earthquake occurrence in Japan. *Earth Planet. Sci. Lett.* **207**, 159–164 (2003). doi:10.1016/S0012-821X(02)01148-2

22. Y. Tanaka, An approximately 9-yr-period variation in seismicity and crustal deformation near the Japan Trench and a consideration of its origin. *Geophys. J. Int.* **196**, 760–787 (2014). doi:10.1093/gji/ggt424

23. F. F. Pollitz, A. Wech, H. Kao, R. Bürgmann, Annual modulation of non-volcanic tremor in northern Cascadia. *J. Geophys. Res. Solid Earth* **118**, 2445–2459 (2013). 10.1002/jgrb.50181 doi:10.1002/jgrb.50181

24. Y. Liu, Numerical simulations on megathrust rupture stabilized under strong dilatancy strengthening in slow slip region. *Geophys. Res. Lett.* **40**, 1311–1316 (2013). 10.1002/grl.50298 doi:10.1002/grl.50298

25. P. Segall, A. M. Rubin, A. M. Bradley, J. R. Rice, Dilatant strengthening as a mechanism for slow slip events. *J. Geophys. Res. Solid Earth* **115**, B12305 (2010). 10.1029/2010JB007449 doi:10.1029/2010JB007449

26. P. Audet, R. Bürgmann, Possible control of subduction zone slow-earthquake periodicity by silica enrichment. *Nature* **510**, 389–392 (2014).

27. R. Hino, D. Inazu, Y. Ohta, Y. Ito, S. Suzuki, T. Iinuma, Y. Osada, M. Kido, H. Fujimoto, Y. Kaneda, Was the 2011 Tohoku-Oki earthquake preceded by aseismic preslip? Examination of seafloor vertical deformation data near the epicenter. *Mar. Geophys. Res.* **35**, 181–190 (2014). doi:10.1007/s11001-013-9208-2

28. S. Ozawa, T. Nishimura, H. Munekane, H. Suito, T. Kobayashi, M. Tobita, T. Imakiire, Preceding, coseismic, and postseismic slips of the 2011 Tohoku earthquake, Japan. *J. Geophys. Res.* **117**, B07404 (2012). 10.1029/2011JB009120 doi:10.1029/2011JB009120

29. T. H. Jordan, L. M. Jones, Operational earthquake forecasting: Some thoughts on why and how. *Seismol. Res. Lett.* **81**, 571–574 (2010). doi:10.1785/gssrl.81.4.571

30. T. Murotani, M. Kikuchi, Y. Yamanaka, "Rupture processes of large Fukushima-Oki earthquakes in 1938," paper S052-004, presented at the 2003 Japan Geoscience Union, Chiba, Japan, 2003.

31. N. Uchida, T. Matsuzawa, W. L. Ellsworth, K. Imanishi, K. Shimamura, A. Hasegawa, Source parameters of microearthquakes on an interplate asperity off Kamaishi, NE Japan over two earthquake cycles. *Geophys. J. Int.* **189**, 999–1014 (2012). 10.1111/j.1365-246X.2012.05377.x doi:10.1111/j.1365-246X.2012.05377.x

32. R. M. Nadeau, L. R. Johnson, Seismological studies at Parkfield VI: Moment release rates and estimates of source parameters for small repeating earthquakes. *Bull. Seismol. Soc. Am.* **88**, 790–814 (1998).

33. T. C. Hanks, H. Kanamori, A moment magnitude scale. *J. Geophys. Res.* **84**, 2348–2350 (1979). 10.1029/JB084iB05p02348 doi:10.1029/JB084iB05p02348

34. K. H. Chen, R. M. Nadeau, R. J. Rau, Towards a universal rule on the recurrence interval scaling of repeating earthquakes? *Geophys. Res. Lett.* **34**, L16308 (2007). doi:10.1029/2007GL030554

35. C. Goltz, D. L. Turcotte, S. G. Abaimov, R. M. Nadeau, N. Uchida, T. Matsuzawa, Rescaled earthquake recurrence time statistics: Application to microrepeaters. *Geophys. J. Int.* **176**, 256–264 (2009). doi:10.1111/j.1365-246X.2008.03999.x

36. T. Igarashi, T. Matsuzawa, A. Hasegawa, Repeating earthquakes and interplate aseismic slip in the northeastern Japan subduction zone. *J. Geophys. Res.* **108**, 2249 (2003). 10.1029/2002JB001920 doi:10.1029/2002JB001920

37. A. P. Mavrommatis, P. Segall, N. Uchida, K. M. Johnson, Long-term acceleration of aseismic slip preceding the Mw 9 Tohoku-oki earthquake: Constraints from repeating earthquakes. *Geophys. Res. Lett.* 2015GL066069 (2015).

38. N. M. Beeler, D. L. Lockner, S. H. Hickman, A simple stick-slip and creep-slip model for repeating earthquakes and its implication for microearthquakes at Parkfield. *Bull. Seismol. Soc. Am.* **91**, 1797–1804 (2001). doi:10.1785/0120000096

39. Y. Suwa, S. Miura, A. Hasegawa, T. Sato, K. Tachibana, Interplate coupling beneath NE Japan inferred from three dimensional displacement field. *J. Geophys. Res.* **111**, 101029/102004JB003203 (2006).

40. A. P. Mavrommatis, P. Segall, K. M. Johnson, A decadal-scale deformation transient prior to the 2011 M_w 9.0 Tohoku-oki earthquake. *Geophys. Res. Lett.* **41**, 4486–4494 (2014). 10.1002/2014gl060139

41. P. Reasenberg, Second-order moment of central California seismicity, 1969–1982. *J. Geophys. Res. Solid Earth* **90**, 5479–5495 (1985). doi:10.1029/JB090iB07p05479

42. G. P. Hayes, D. J. Wald, R. L. Johnson, Slab1.0: A three-dimensional model of global subduction zone geometries. *J. Geophys. Res. Solid Earth* **117**, B01302 (2012). 10.1029/2011JB008524